Title

Investigating impacts of forest fires in Alaska and western Canada on regional weather over the northeastern United States using CAM5 global simulations to constrain transport to a WRF-Chem regional domain

Journal

Journal of Geophysical Research: Atmospheres, 119(12)

ISSN

2169-897X

Authors

Zhao, Zhan
Kooperman, Gabriel J
Pritchard, Michael S
et al.

Publication Date

2014-06-27

DOI

10.1002/2013jd020973

AGU PUBLICATIONS

JGR

Journal of Geophysical Research: Atmospheres

RESEARCH ARTICLE
10.1002/2013JD020973

Key Points:
- Nonlocal fire emissions resulted in ~10% precipitation reduction
- Nonlocal fire emissions reduced peak surface shortwave radiation at by 25 W m^{-2}
- An aerosol-enabled globally driven regional modeling system is developed

Correspondence to:
L. M. Russell,
lmrussell@ucsd.edu

Citation:
Zhao, Z., G. J. Kooperman, M. S. Pritchard, L. M. Russell, and R. C. J. Somerville (2014), Investigating impacts of forest fires in Alaska and western Canada on regional weather over the northeastern United States using CAM5 global simulations to constrain transport to a WRF-Chem regional domain, *J. Geophys. Res. Atmos.*, *119*, 7515–7536, doi:10.1002/2013JD020973.

Received 15 OCT 2013
Accepted 27 MAY 2014
Accepted article online 2 JUN 2014
Published online 18 JUN 2014

Investigating impacts of forest fires in Alaska and western Canada on regional weather over the northeastern United States using CAM5 global simulations to constrain transport to a WRF-Chem regional domain

Zhan Zhao[1,2], Gabriel J. Kooperman[1,3], Michael S. Pritchard[1,3], Lynn M. Russell[1], and Richard C. J. Somerville[1]

[1]Scripps Institution of Oceanography, University of California, San Diego, La Jolla, California, USA, [2]Now at Air Quality and Planning Science Division, California Air Resources Board, Sacramento, California, USA, [3]Now at Department of Earth System Science, University of California, Irvine, California, USA

Abstract An aerosol-enabled globally driven regional modeling system has been developed by coupling the National Center for Atmospheric Research's Community Atmosphere Model version 5 (CAM5) with the Weather Research and Forecasting model with chemistry (WRF-Chem). In this modeling system, aerosol-enabled CAM5, a state-of-the-art global climate model is downscaled to provide coherent meteorological and chemical boundary conditions for regional WRF-Chem simulations. Aerosol particle emissions originating outside the WRF-Chem domain can be a potentially important nonlocal aerosol source. As a test case, the potential impacts of nonlocal forest fire aerosols on regional precipitation and radiation were investigated over the northeastern United States during the summer of 2004. During this period, forest fires in Alaska and western Canada lofted aerosol particles into the midtroposphere, which were advected across the United States. WRF-Chem simulations that included nonlocal biomass burning aerosols had domain-mean aerosol optical depths that were nearly three times higher than those without, which reduced peak downwelling domain-mean shortwave radiation at the surface by ~25 W m^{-2}. In this classic twin experiment design, adding nonlocal fire plume led to near-surface cooling and changes in cloud vertical distribution, while variations in domain-mean cloud liquid water path were negligible. The higher aerosol concentrations in the simulation with the fire plume resulted in a ~10% reduction in domain-mean precipitation coincident with an ~8% decrease in domain-mean CAPE. A suite of simulations was also conducted to explore sensitivities of meteorological feedbacks to the ratio of black carbon to total plume aerosols, as well as to overall plume concentrations. Results from this ensemble revealed that plume-induced near-surface cooling and CAPE reduction occur in a wide range of conditions. The response of moist convection was very complex because of strong thermodynamic internal variability.

1. Introduction

Biomass burning significantly affects climate and air quality by providing a major source of greenhouse gases and carbonaceous aerosols, including black carbon and organic carbon [*Seiler and Crutzen*, 1980; *Crutzen and Andreae*, 1990]. Black carbon and organic carbon not only interact with solar radiation via the aerosol direct effect [*Penner et al.*, 1992; *Intergovernmental Panel on Climate Change*, 2007] but also serve as cloud condensation nuclei (CCN) to affect clouds and precipitation via the aerosol indirect effect [*Twomey*, 1974; *Albrecht*, 1989; *Kaufman and Fraser*, 1997; *Roberts et al.*, 2003]. Aerosol particles and trace gases from wildfires with a relatively high-injection height are subject to long range transport, affecting regional air quality and meteorological conditions far away from emission sources. For instance, emissions from boreal wildfires in Alaska and western Canada have often been detected over the eastern United States about 1 week after the fire event during summertime [*Wotawa and Trainer*, 2000; *Colarco et al.*, 2004; *Warneke et al.*, 2006].

During the summer of 2004, extreme drought conditions over Alaska and western Canada led to extensive wildfires burning across these regions [*Turquety et al.*, 2007; *Pfister et al.*, 2008]. Burned areas over Alaska

were about 10 times greater than 10 year averages [*Stohl et al*., 2006]. Satellite images from Measurements of Pollutions in the Troposphere (MOPITT), Geostationary Operational Environmental Satellite (GOES), and Atmospheric Infrared Sounder indicated a significant amount of forest fire aerosols from Alaska and western Canada transported to the northeastern United States in both the boundary layer and free troposphere [*Pfister et al*., 2005]. Also, at this time, the International Consortium for Atmospheric Research on Transport and Transformation (ICARTT) field campaign was conducted over North America and Europe to focus on atmospheric chemistry and transport [*Fehsenfeld et al*., 2006]. Several ICARTT flights encountered fire plumes over the eastern United States that originated from Alaska and western Canada in both the boundary layer and free troposphere [*McMillan et al*., 2008].

The Weather Research and Forecasting model (WRF) with Chemistry (WRF-Chem) [*Grell et al*., 2005], a fully coupled meteorology-chemistry model, has previously been employed to study the impacts of *local* biomass burning aerosols on regional meteorological conditions. For example, *Grell et al*. [2011] found that during summer 2004, wildfires over Alaska led to a shallower and moister boundary layer in cloud-free areas during daytime due to a strong aerosol direct effect; in contrast, in areas with convection, smoke suppressed precipitation during stratiform convective regimes (e.g., at night when clouds were nonconvective with low altitude) but enhanced convection in the afternoon when precipitation was convective. Interestingly, an opposite effect was reported by *Wu et al*. [2011], who simulated a biomass burning event over South America and reported that smoke aerosols led to a decrease in clouds and precipitation in the afternoon but an increase in these conditions at night. *Wu et al*. [2011] employed two horizontal resolutions (36 km—parameterized convection and 4 km—convection resolving). Their results showed that the overall decrease in surface precipitation was greater in the simulation with a 36 km resolution (5% decrease) than the simulation with a 4 km resolution (3% decrease). The aerosol indirect effects played a stronger role in the simulation with a 4 km resolution than the counterpart with a 36 km resolution, because the aerosol indirect effects in WRF-Chem are not allowed by the convective parameterization that was employed in the simulation with a 36 km resolution. The differences in the precipitation response in the two WRF-Chem simulations in *Wu et al*. [2011] are likely the result of this lack of aerosol indirect effect in the convective parameterization for the domain with a 36 km resolution.

These studies only focused on the meteorological impacts of biomass burning aerosols emitted within the WRF-Chem domain. It is difficult to examine the impacts of aerosols emitted from *nonlocal* sources in conventional regional WRF-Chem simulations, for example to investigate the influence of trans-Pacific pollutants emitted from Asia on the meteorological and air quality conditions over the western U.S. In coupled meteorology-chemistry models, such as WRF-Chem, pollutants emitted outside of the model domain flow into the regional domain via lateral boundaries. Long-range transported wildfire pollutants can contribute significantly to chemical and meteorological conditions in regional model simulations. *Zhao et al*. [2012] investigated potential impacts of long-range transported biomass burning aerosols on convective systems far away from emission sources by introducing idealized smoke plumes (a mixture of sulfate at 6 $\mu g\,m^{-3}$ and black carbon at 1 $\mu g\,m^{-3}$) along the WRF-Chem lateral boundary at different altitudes. Results from that study suggested that the altitude of the fire plume at the upstream boundary was an important factor determining their impacts on a convective system as a plume introduced at 1.5 to 2.5 km altitude led to optically thicker clouds and a ~30% decrease in surface precipitation.

Investigating the influence of nonlocal aerosol inflow in regional air quality simulations is currently an area of active research. *Huang et al*. [2010] reported the importance of characterizing the vertical structure of chemical boundary conditions in summertime ozone simulations over California. WRF-Chem simulation in *Pfister et al*. [2011] suggested that pollutant inflows at model lateral boundaries could significantly influence surface air quality in the modeled regional domain over California. Typically, regional air quality studies that focused on aerosols emitted within the model domain have used temporal-spatial invariant background profiles that represent either mean conditions for the simulation period [*Winner et al*., 1995; *Fast et al*., 2006] or typical clean conditions [*Grell et al*., 2011; *Sessions et al*., 2010] as lateral boundary conditions for the chemical components. Recent studies have employed time-dependent chemical boundary conditions derived from a global chemical transport model (GCTM) to represent external pollutant plumes entering the regional domain through the lateral boundaries [*Fast et al*., 2009; *Lin et al*., 2010; *Pfister et al*., 2011; *Saide et al*., 2012; *Tang et al*., 2004]. Meteorological boundary conditions for the

regional model were derived from analysis or a global climate model (GCM), while chemical boundary conditions were derived from another GCTM in these studies.

A limitation of the aforementioned modeling approach is its inability to extend to future climate scenarios, since conventional GCTMs depend on observed dynamics. A framework is developed in this study with both meteorological and chemical boundary conditions of WRF-Chem derived from a single aerosol-enabled global climate model (AE-GCM)—the National Center for Atmospheric Research's (NCAR) aerosol-enabled Community Atmosphere Model version 5 (CAM5) [*Neale et al*., 2010]. This new type of framework provides a link between research investigating the regional meteorological/air quality impact and the global-scale perturbations of climate models. Moreover, this type of modeling framework can be integrated for decades into the future to explore potentially interesting sensitivities of regional meteorology and air quality to global-scale changes in emissions and climate. Here we use this modeling framework to explore the potential impacts of wildfire emissions in Alaska and western Canada on meteorological conditions—especially convective systems—over the northeastern United States during a summer 2004 boreal forest fire plume transport event. It should be noted that when compared with conventional downscaling, additional steps are needed in order to downscale the chemical variables, and for this reason we identify this process as downscaling with chemical coupling. Both aerosol-radiation and aerosol-cloud interactions were represented in CAM5, which was run in an observation-constrained mode by "nudging" (details in section 3.1) the simulation toward observed meteorological conditions. Nudging forces CAM5 to reproduce observed synoptic plume transport pathways during this period, which carry transient biomass burning aerosols to WRF-Chem's lateral boundaries. This modeling framework provides an opportunity to include coherent meteorological and chemical lateral boundary conditions in the regional model domain where convection is simulated explicitly, despite the fact that some inconsistencies remain between CAM5 and WRF-Chem since they use different representations of the aerosol size distribution and have different meteorological parameterizations and grid structure.

The upcoming analysis focuses on the impacts of long-range transported wildfire aerosols on convective systems and vertical profiles of temperature and moisture, as well as the wet scavenging of plume aerosols by the convective system. Moreover, a sensitivity test is conducted to probe atmospheric responses to fire plumes with different ratios of black carbon to other plume aerosols. Model descriptions and development of the interface between WRF-Chem and CAM5 are documented in section 2. Section 3 describes the experimental design. Results, including the impacts of the fire plume on the convective system, solar radiation, temperature, wet scavenging of plume aerosols, as well as a sensitivity test by varying plume intensity and composition, are presented in section 4. Section 5 provides a summary.

2. Model Descriptions and the Interface

2.1. WRF-Chem Model Description

The regional component of this modeling system, WRF-Chem Version 3.2, is the chemistry version of WRF [*Skamarock et al*., 2008], a nonhydrostatic mesoscale model widely used for both research and operational purposes. Meteorology and chemistry are fully coupled in WRF-Chem. Both aerosol-radiation interaction [*Fast et al*., 2006] and aerosol-cloud-radiation interaction [*Chapman et al*., 2009] are implemented in WRF-Chem. In-cloud and below-cloud wet scavenging of aerosols are also considered. These treatments make WRF-Chem a state-of-the-art numerical test bed to investigate interactions between aerosols and meteorological parameters, such as clouds and precipitation.

2.2. CAM5 Model Description

CAM5 is the global component of this modeling system. CAM5 includes interactive aerosol-cloud physical pathways, through parameterizations for both aerosol direct effects and indirect effects on cloud droplet formation and the thermodynamic structure of the atmosphere [*Neale et al*., 2010]. An interactive three-mode (Aitken, accumulation, and coarse) aerosol module transports and processes 15 different aerosol constituents as they evolve through nucleation, growth by condensation, coagulation, aqueous-phase production, and removal by wet and dry deposition [*Liu et al*., 2012].

2.3. Interface Between CAM5 and WRF-Chem

An interface was developed so that coherent meteorological and chemical lateral boundary conditions for WRF-Chem could be obtained from CAM5 simulation results. The development of the meteorological part of the interface was based on the method described by *Zhao et al*. [2011]. Three-dimensional CAM5 meteorological fields treated in this interface provided WRF-Chem lateral boundaries including temperature, wind, geopotential height, humidity, and mixing ratios of hydrometers (cloud, ice, rain, snow, and graupel). Two-dimensional CAM5 meteorological variables used as lateral boundaries for WRF-Chem included surface pressure, sea level pressure, skin temperature, terrain height, 2 m temperature, surface temperature, sea surface temperature, and ice fractions. In addition, within this interface CLM4 provided soil temperature, soil moisture, land-sea mask, 2 m moisture, and water equivalent snow depth for WRF-Chem.

The development of the chemistry part of the interface was based on the code "mozbc" developed at NCAR's Atmospheric Chemistry Division (https://www2.acd.ucar.edu/), which has been used to create time-varying chemical boundary conditions for WRF-Chem from the Model for Ozone and Related chemical Tracers (MOZART) global model output. Several modifications were made to the code due to differences in chemical species and aerosol treatments between CAM5 and MOZART. WRF-Chem's aerosol treatment was configured for consistency with CAM5, i.e., the Modal Aerosol Dynamics Model for Europe Secondary Organic Aerosol Model (MADE/SORGAM) aerosol module was selected, which also uses three modes (Aitken, accumulation, and coarse mode) to represent aerosol size distributions. Internal mixing is assumed for aerosols within each mode of the MADE/SORGAM aerosol module. Note that although a modal distribution and three modes aerosol distribution were used in both CAM5 and WRF-Chem, the characteristics of the modes in the two aerosol treatments are slightly different. MADE/SORGAM uses a relatively old treatment of secondary organic aerosol (SOA) and produces very little SOA compared to observations. Thus, aerosol aging may be underestimated in the WRF-Chem simulations. CAM5 aerosols treated in the interface included concentrations of black carbon, dust, sea salt, sulfate, primary and secondary SOA, as well as total aerosol number concentrations. Sea salt aerosols in CAM5 were partitioned to derive sodium and chloride for WRF-Chem, assuming that 31% (55%) of sea salt mass was sodium (chloride) based on *Lewis and Schwartz* [2004]. Instead of predicting both ammonium and sulfate aerosols as in WRF-Chem, the aerosol module in CAM5 predicts the mass mixing ratio of sulfate aerosols in the form of ammonium bisulfate (NH4HSO4) [*Neale et al*., 2010]. Therefore, the mixing ratio of ammonium is calculated based on the mass mixing ratio of sulfate aerosols from CAM5 and the molar mass composition of ammonium bisulfate. CAM5 has only one SOA species, but there are several SOA species in the MADE/SORGAM aerosol module in WRF-Chem. In this interface, SOA in CAM5 is mapped to anthropogenic organics from alkanes only, and other SOA species in MADE/SORGAM are not used.

3. Experimental Design

3.1. CAM5 Configuration

To examine the impact of fire emissions on meteorological and chemical conditions over the northeastern United States, it was critical that CAM5 simulated the observed circulation and aerosol emissions that occurred during the ICARTT field campaign. This was accomplished by (a) "nudging" to observationally constrain the global model and (b) incorporating high time-resolution forest fire emissions (which is not common for a climate model).

3.1.1. Nudging

A Newtonian relaxation technique was incorporated into CAM5's physics package in which the model's winds and temperature were nudged toward a best estimate of the atmospheric state, as obtained from the European Centre for Medium-Range Weather Forecasts (ECMWF) ERA-Interim reanalysis, which provides model level atmospheric analysis fields at 6 h time resolution and T255 horizontal spectral resolution with 60 vertical levels [*Dee et al*., 2011]. CAM5 in this experiment was configured with 1.9° latitude by 2.5° longitude horizontal resolution and 30 hybrid vertical levels, so careful consideration was given to regrid ERA-Interim reanalysis to avoid model inconsistencies. The nudging and regridding procedure implemented here was adapted from current best practices at NCAR largely stemming from experience with an earlier version of CAM (2/3) used for initializing forecast simulations to evaluate the growth of climate model errors on short time scales [e.g., *Boyle et al*., 2005]. Spatial interpolation accounts for area-conserving horizontal

remapping, surface pressure, and field-specific vertical adjustment to topographic differences between CAM and the reanalysis model, as well as removal of spurious supersaturation resulting from the interpolation of temperature. Temporal cubic interpolation to the model's 30 min time step occurs internally within the model, and the nudging is applied with a 6 h relaxation time scale. This relaxation time was chosen because it (1) matched the 6 h resolution of ECMWF, (2) kept the magnitude of the nudging tendency comparable to tendencies derived from physical parameterizations, and (3) did not dramatically alter unconstrained model fields, so that CAM5 behaved similarly to free-running mode while still constraining large-scale circulation and meteorology. The simulations were continuously nudged for 9 months toward ECMWF horizontal winds and dry static energy, but the first 6 months were excluded from analysis and treated as model spin-up. More discussion of nudging and its effects on CAM5 is provided in *Kooperman et al*. [2012].

3.1.2. Emissions

The present-day aerosol emission datasets in CAM5 include anthropogenic emissions based on year 2000 conditions and multiyear averaged monthly biomass burning emissions [*Neale et al*., 2010; *Lamarque et al*., 2010]. Since multiyear monthly averages are unable to represent transient emission plume structures from individual fires, daily emission estimates from the Global Fire Emission Database Version 3 (GFEDv3) were used to create emission files for this experiment [*Van der Werf et al*., 2010; *Mu et al*., 2011]. The GFEDv3 data set provide total column burdens for black carbon, organic carbon, sulfate, and sulfur dioxide at $0.5° \times 0.5°$ resolution, as estimated from Moderate Resolution Imaging Spectroradiometer (MODIS) burned area retrievals and modeled vegetation fuel loads [*Giglio et al*., 2010]. These estimates were mapped to the CAM5 grid using area-conserving horizontal interpolation and vertical injection heights distributed into CAM5 levels based on the method employed by *Turquety et al*. [2007].

The injection height of fire emissions is crucial for long-range plume transport [*Colarco et al*., 2004; *Turquety et al*., 2007] because, in most cases, only fire emissions injected well above the boundary layer are subject to long-range transport. *Turquety et al*. [2007] tested several assumptions for injection height in GEOS-Chem simulations for the transport of fire emissions from Alaska and Western Canada to the eastern United States during the summer of 2004. They found that their model results matched MOPITT satellite observations best when injecting 40% of the total emissions into the boundary layer, 30% from the top of the boundary layer to 400 hPa, and 30% from 400 to 200 hPa. In this study we mimicked their injection strategy but acknowledge that this aspect of transient plume injection is a source of potential systematic error since independent satellite estimates suggest only 15% of emissions are injected above the boundary layer [*Val Martin et al*., 2010].

CAM5 was run in this experiment as a standalone atmospheric model with interactive land (from the Community Land Model; CLM4) but prescribed sea surface temperatures and sea ice from the Hadley Centre dataset. The two-moment cloud microphysics scheme by *Morrison and Gettelman* [2008] is used in CAM5 simulations. Deep and shallow convection parameterizations are based on *Zhang and McFarlane* [1995] and *Park and Bretherton* [2009], respectively, which approximate unresolved vertical fluxes of mass and energy, including the vertical transport of interstitial and cloud-borne aerosol particles. Two CAM5 simulations were conducted in this study: one with the daily fire emissions included (CAM_GFED) and one with no fire emissions (CAM_NoFire; fire emissions were removed from CAM5 standard emissions).

3.2. WRF-Chem Configurations and Simulations

WRF-Chem was configured with three nested domains using horizontal resolutions of 27, 9, and 3 km (Figure 1). All domains had 35 vertical layers, from the surface to 100 mbar. The lowest eight layers were contained in the first kilometer above the surface to capture atmospheric processes within the boundary layer, which are essential to the formation and evolution of convective systems. MADE/SORGAM aerosol module is used to be consistent with the aerosol treatment in CAM5. Other selected configuration options for physical and chemical processes were the same as those applied in *Zhao et al*. [2012]. Lin microphysics was employed for all three domains. WRF-Chem resolves convective eddies explicitly only when the horizontal resolution is less than 5 km [*Skamarock et al*., 2008]. Therefore, the Grell three-dimensional convective parameterization [*Grell and Devenyi*, 2002] was applied to the two outer domains to represent subgrid-scale convective systems that were not resolved by Lin microphysics due to their relatively coarse spatial resolution. The innermost domain (3 km resolution) was left to "resolve" convection explicitly. Lin microphysics applied in the study is a two-moment scheme because a prognostic treatment of cloud droplet

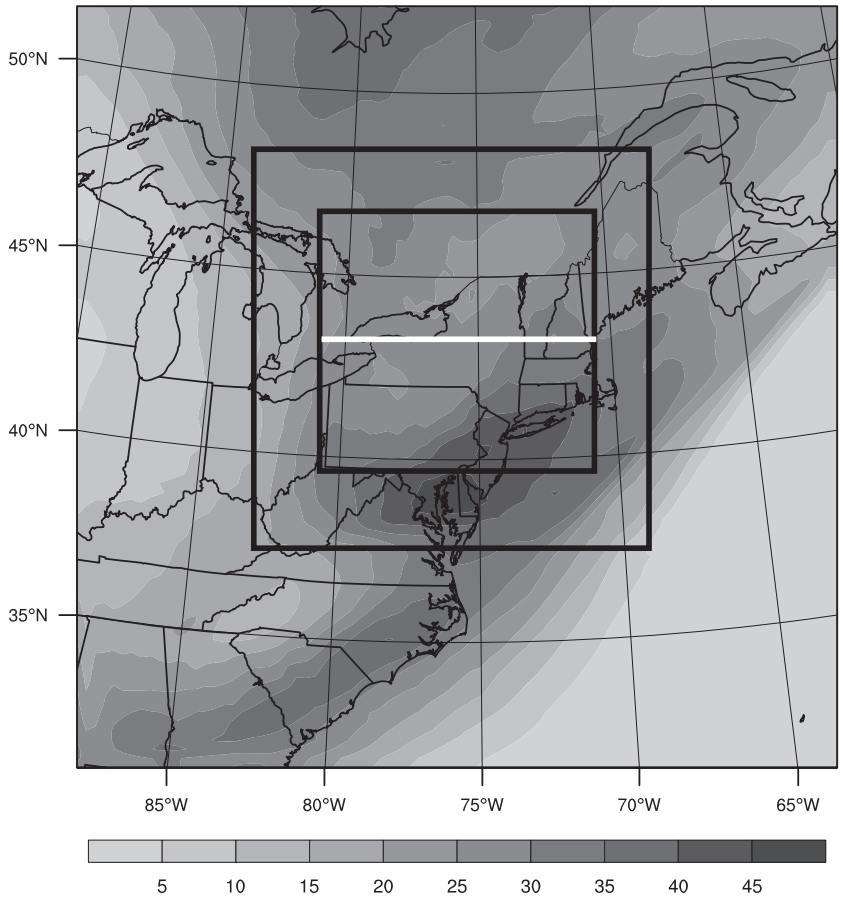

Figure 1. WRF-Chem nested domain and the difference of $PM_{2.5}$ total column burden ($mg\,m^{-2}$) from FIRE simulation relative to NoFIRE temporally averaged for 21 and 22 July 2004. The white line in the innermost domain indicates location of the vertical cross section in Figure 9.

number was added to the Lin microphysics [*Chapman et al.*, 2009; *Ghan et al.*, 1997]. The autoconversion rate for cloud droplets forming rain droplets depends on both prognostic cloud water mass and cloud droplet number concentration in this two-moment Lin microphysics [*Liu et al.*, 2005; *Lin et al.*, 1983]. The cloud droplet number concentration is also linked to the shortwave radiation calculation, which affects incoming solar radiation. Note that the aerosol indirect effect is only treated for liquid clouds that are resolved by the microphysics scheme. Thus, within the outer two domains, aerosol-cloud interactions were only considered for the part of the clouds associated with Lin microphysics. The longwave radiation effect of aerosols was not implemented in the version of WRF-Chem used in this study. Interaction between aerosols and shortwave radiation is considered in all three domains. Aerosol-cloud interactions were coupled only with Lin microphysics in WRF-Chem V3.2, which is the version applied in this study. More comprehensive microphysics schemes, such as the Morrison scheme [*Morrison et al.*, 2009], that are also coupled with aerosol-cloud interactions in the latest version of WRF-Chem (V3.5) should be considered for later studies.

Comparison of results from CAM_GFED and CAM_NoFire (not shown) indicated that the fire plumes originated primarily from Alaska and Western Canada fires and had been transported into the WRF-Chem domain (Figure 1). A series of 5 day WRF-Chem simulations were conducted, each initialized on 18 July 2004 00:00 UTC and ran through 23 July 2004 00:00 UTC, to coincide with the arrival of forest fire aerosols emitted from Alaska and western Canada at the innermost WRF-Chem domain based on CAM_GFED simulation results. The effects of the nonlocal source fire aerosols on a precipitating convective system that developed within the innermost WRF-Chem domain during this period are of primary scientific interest in this study. Hourly anthropogenic aerosol and gas-phase local emissions within the WRF-Chem domains were based on the U.S. Environmental Protection Agency (EPA)'s National Emission Inventory 2005 (NEI-05). Land use based

Table 1. Meteorological Lateral Boundary Conditions, Chemical Lateral Boundary Conditions, and Aerosol Effects Activated for Each WRF-Chem Simulation

	Meterological Lateral Boundary Conditions	Chemical Lateral Boundary Conditions	Aerosol-cloud interaction	Aerosol-radiation interaction
FIRE	CAM_GFED	CAM_GFED	On	On
NoFIRE	CAM_NoFire	CAM_NoFire	On	On
CAM_driven	CAM_NoFire	Idealized profiles	On	On
NARR_driven	NARR	Idealized profiles	On	On

biogenic emissions were used following the Guenther scheme [*Guenther et al*., 1993]. Sea salt and dust emissions were also based on land use information and the simulated meteorological fields. Simulation results prior to 21 July 2004 00:00 UTC were considered as model spin-up and our analysis and discussion focused on results from the final 2 days of the simulation.

Six WRF-Chem simulations were carried out with different lateral boundary conditions and aerosol physics configurations (Table 1). Meteorological and chemical boundary conditions for simulation FIRE and NoFIRE were derived from CAM_GFED and CAM_NoFire simulation results, respectively. These two simulations were designed to infer the overall impacts of these long-range transported fire plumes on the simulated convective systems. CAM_driven and NARR_driven simulations (Table 1) were designed to evaluate the performance of this CAM5 and WRF-Chem modeling framework. Both simulations used a vertical profile for each gas phase and aerosol species, which represent clean background midlatitude conditions in the Northern Hemisphere [*Liu et al*., 1996], as chemical boundary conditions. Meteorological boundary conditions for CAM_driven and NARR_driven were obtained from CAM_NoFire simulation results and North American Regional Reanalysis (NARR) [*Mesinger et al*., 2006], respectively. The NARR data sets with a 32 km horizontal resolution assimilated many observations including satellite and conventional upper air and surface data and, in general, matched observations well. Thus, NARR_driven was used as a qualitative benchmark to examine the performance of this modeling framework.

Although default fire emissions in CAM5 were replaced with daily GFED fire emissions, all other CAM5 emissions were based on year 2000 monthly mean emissions [*Lamarque et al*., 2010], and all WRF-Chem emissions were based on hourly EPA's NEI-05 that represent a typical ozone season day. Therefore, local emissions applied to this study can be considerably different from real conditions and from each other, which is one source of potential error in the apparent impacts of the transported aerosols. Furthermore, we employed an idealized injection height for wildfire emissions based on a previous study; thus, in this study, significant discrepancies might exist in the transport altitudes and plume intensity of the fire plume relative to reality. Moreover, interactions between aerosols and ice nuclei is only included in the global component (CAM5) of this modeling framework. There is also the issue of horizontal resolution, which is limited by computational resources to 3 km, and thus, our model does not explicitly capture the smaller scales of turbulence relevant to the physics of shallow convective systems. Finally, internal atmospheric variability is an inherent source of potential error in this sort of modeling investigation.

4. Results and Discussion

4.1. Verification of the Modeling Framework

Figures 2 and 3 demonstrate that the techniques applied to observationally constrain CAM5 and to use the resulting simulations as boundary conditions for WRF/Chem were self-consistent and comparable to observations. Figure 2 compares the simulated precipitation pattern of the coupled modeling framework (CAM_driven) with that of the WRF-Chem simulation driven by a typical supported forcing, the NARR reanalysis (NARR_driven). Some precipitation differences between CAM_driven (Figure 2a) and NARR_driven (Figure 2b) were obvious both over the ocean and over land, which likely resulted from discrepancies in the representation of the synoptic weather system between the two simulations (Figures 3a and 3b). Simulated precipitation over the ocean, in connection with rising motion east of the upper level trough, was captured in both CAM_driven and NARR_driven simulations (Figures 3a and 3b). However, the orientation and strength of this upper level trough, potentially key factors in surface rainfall patterns [*Zangvil and Druian*, 1990; *Ritchie and Elsberry*, 2007], differed in the two simulations and was shifted to the east in the

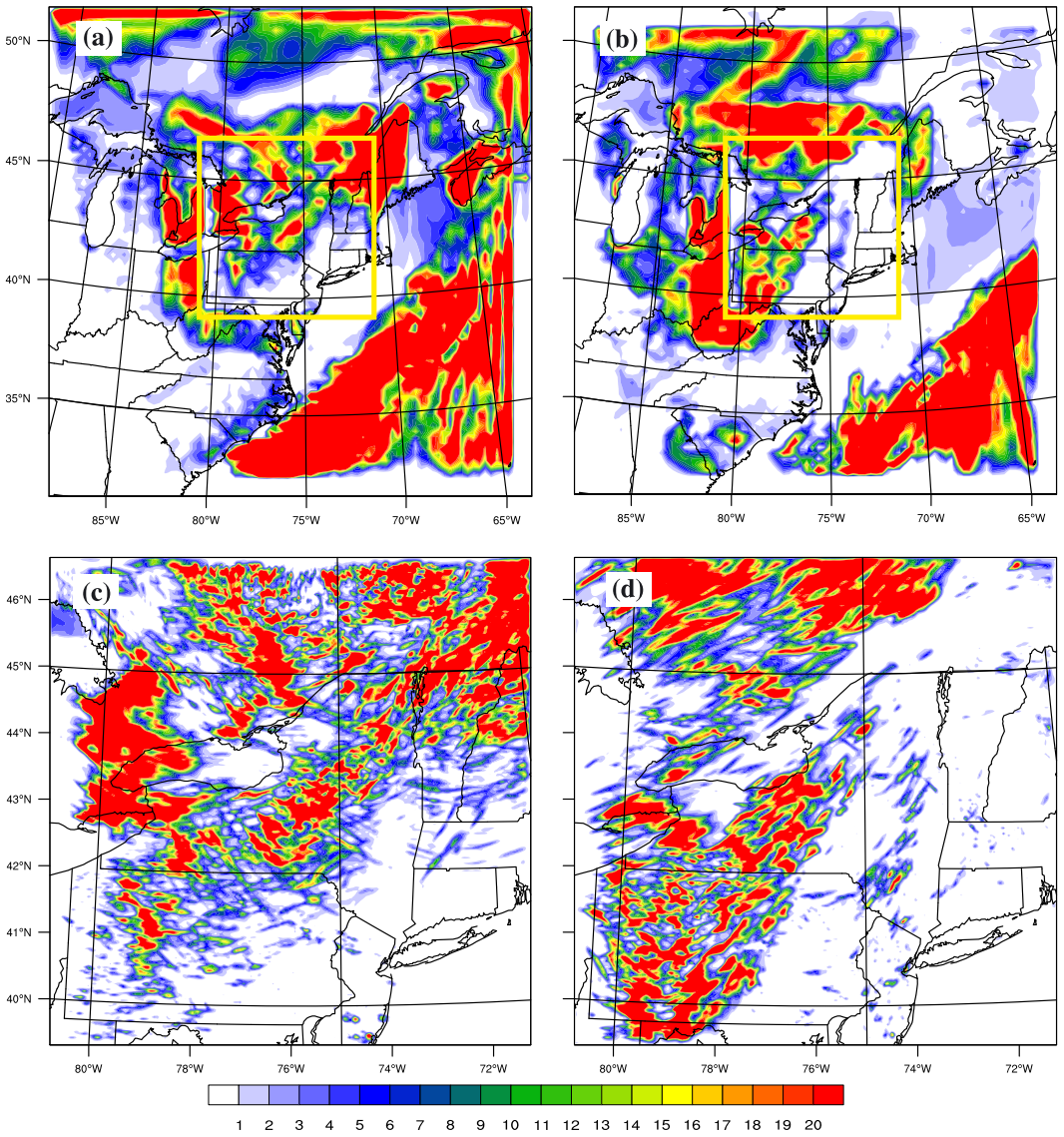

Figure 2. Total precipitation (mm) during the 2 day simulation period for the outermost WRF-Chem domain from (a) CAM_driven and (b) NARR_driven, and for the innermost WRF-Chem domain from (c) CAM_driven and (d) NARR_driven. Yellow boxes in Figures 2a and 2b indicate the region represented in Figures 2c and 2d.

NARR_driven simulation (Figures 3a and 3b). Discrepancies in the precipitation over land may also be related to the orientation and strength of the trough. Rainfall patterns in the innermost WRF-Chem domain with explicit convection were qualitatively consistent between the two simulations (Figures 2c and 2d). Although a larger area of the domain was covered with precipitation in CAM_driven (Figure 2c) compared to NARR_driven (Figure 2d). Precipitation within the innermost domain (Figures 2c and 2d) was in the southeast part of the large convective system covering the northeastern United States (Figures 2a and 2b). Thus, discrepancies in rainfall patterns between CAM_driven (Figure 2c) and NARR_driven (Figure 2d) were, at least partially, due to the imprecise prediction of this large convective system from the coupled model simulation (CAM_driven). Such discrepancies show the considerable sensitivity of resolved convection to changes in external forcing, illustrating that the internal variability within WRF/Chem also contributes to the differences between simulations.

The synoptic pattern from the coupled model (Figure 3a—WRF-Chem outermost domain) and the original CAM5 simulation (Figure 3c—global model) correspond closely to each other, suggesting that the

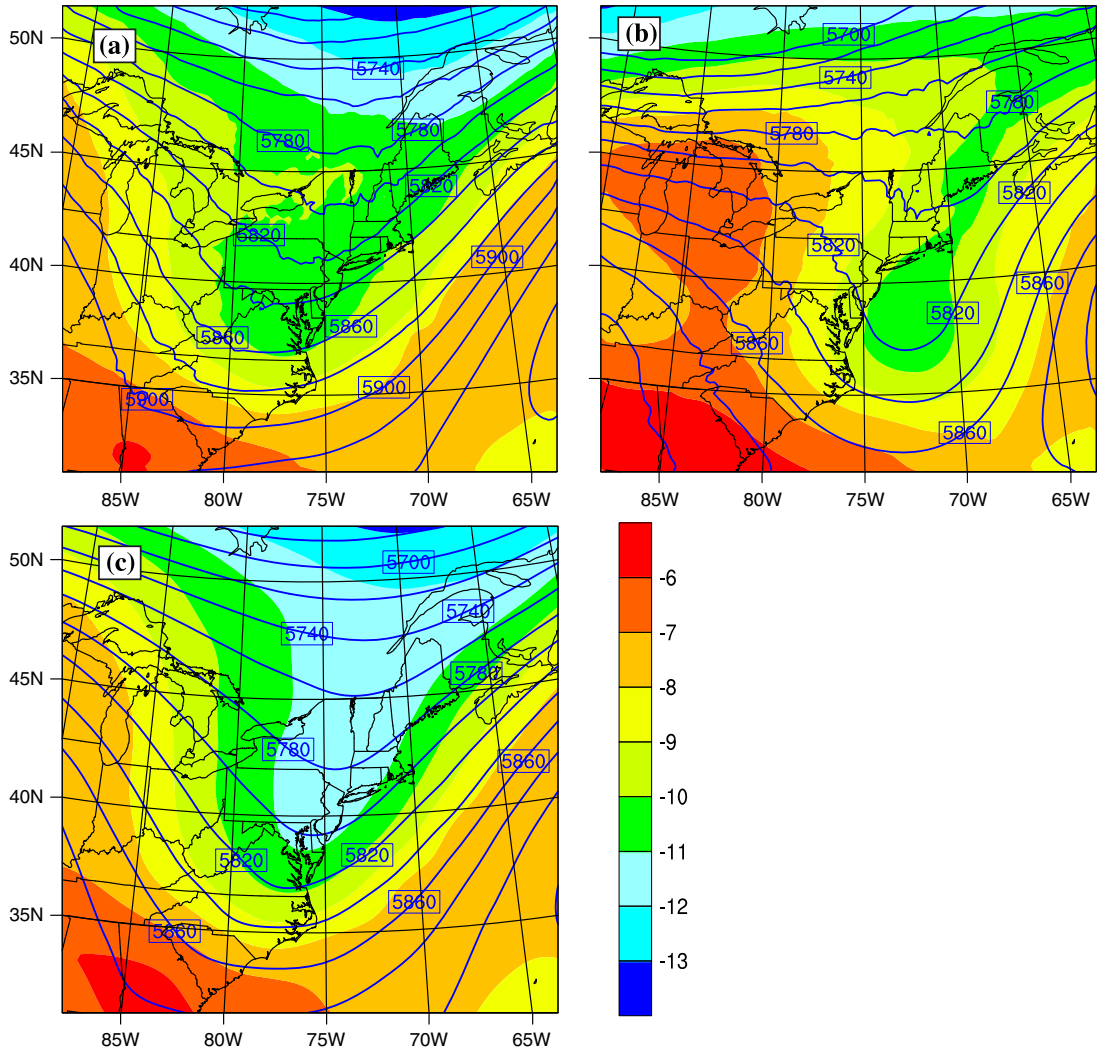

Figure 3. Two day mean 500 mbar temperature (colors; in °C) overlaid with geopotential height (blue contours; in meters) for (a) CAM_driven, (b) NARR_driven, and (c) CAM_NoFire simulation. Note that Figures 3a and 3b are for WRF-Chem results from the outmost domain with 27 km horizontal resolution; CAM5 result were regridded to WRF-Chem 27 km grids in Figure 3c for comparison purpose.

coupling between the two models was successful. There is also good agreement between the two simulations in atmospheric fields at 850 mbar (temperature and geopotential height) and at the surface (2 m temperature and sea level pressure) (not shown). However, there are noticeable differences in small-scale features including a slightly higher (~1°K) temperature in the coupled model (Figure 3a) over the northeastern United States. These differences demonstrate that WRF-Chem is not completely constrained by the coupling during the simulation period even though CAM5 provided lateral boundary conditions and the nudging field to the outermost domain at a 6 h time scale.

4.2. Comparison of Model Results to Observations

The Particle Soot Absorption Photometer (PSAP) on board the NASA DC-8 aircraft during the ICARTT field campaign [*Fehsenfeld et al.*, 2006] measured the aerosol light absorption at 660 nm (in m^{-1}), which is converted into a nominal black carbon concentration using an assumed mass absorption efficiency of $6.6 \pm 1\ m^2\ g^{-1}$ based on *Chow et al.* [2009]. The standard error is meant to reflect possible sources of uncertainty.

In order to evaluate CAM_GFED output relative to PSAP aircraft measurements, a colocated model black carbon profile was calculated for flights that occurred near the interior of the WRF-Chem domain. All

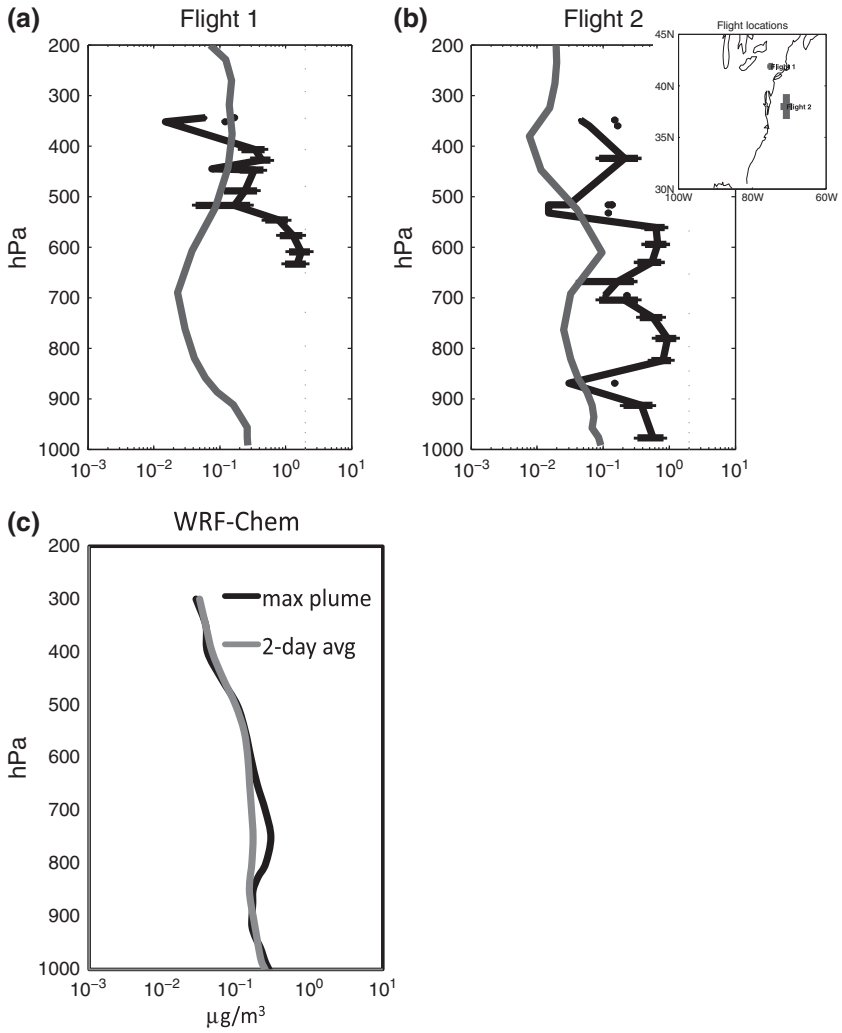

Figure 4. (a–c) Profiles of observed (black) versus CAM_GFED simulated (grey) black carbon concentration (in log scale). Model output is colocated in space and time with two ICARTT flight paths whose horizontal footprints are shown in the inset legend in Figure 4b. Figure 4c shows WRF-Chem-simulated black carbon vertical profile averaged over the CAM5 grid cell used in Figure 4a averaged over the 2 day simulation period (grey) and at the hour with the maximum plume concentration (black).

CAM5 grid columns located within 1 standard deviation of the mean horizontal flight position were analyzed. Flight 1 took place between 21:16 and 21:31 UTC on 20 July, and flight 2 took place between 13:42 UTC and 14:30 UTC on 22 July. This intercomparison is shown in Figure 4. Elevated black carbon concentration between 400 to 500 mbar (500 to 700 mbar) in both observed and CAM5 simulated profiles in Figure 4a (Figure 4b) demonstrated that the aerosol concentration in CAM5 replicates some of the key plume features; however, the intensity of the fire plume was greatly underestimated in CAM5 by 1–2 orders of magnitude depending on the elevation. The first reason for this underestimation is the temporal and spatial scale mismatch between an instantaneous in situ flight and a 3 h average of CAM results with $1.9 \times 2.5°$ resolution, where the latter dilutes the plume concentrations substantially. Overestimation of particle losses during transport by CAM5 could also contribute to the underestimation of black carbon concentration. This discrepancy may also reflect underestimated emissions [*Zhao et al.*, 2010], since offline comparison (not shown) suggests that wildfire smoke over the fire source region is approximately 50% lower in the simulated aerosol optical depth (AOD) than in the MODIS-observed AOD, consistent with findings that GFEDv3 may underestimate actual column wildfire emissions [*Stroppiana et al.*, 2010]. More detailed comparisons of CAM5 results to observations are the focus of another paper (in preparation).

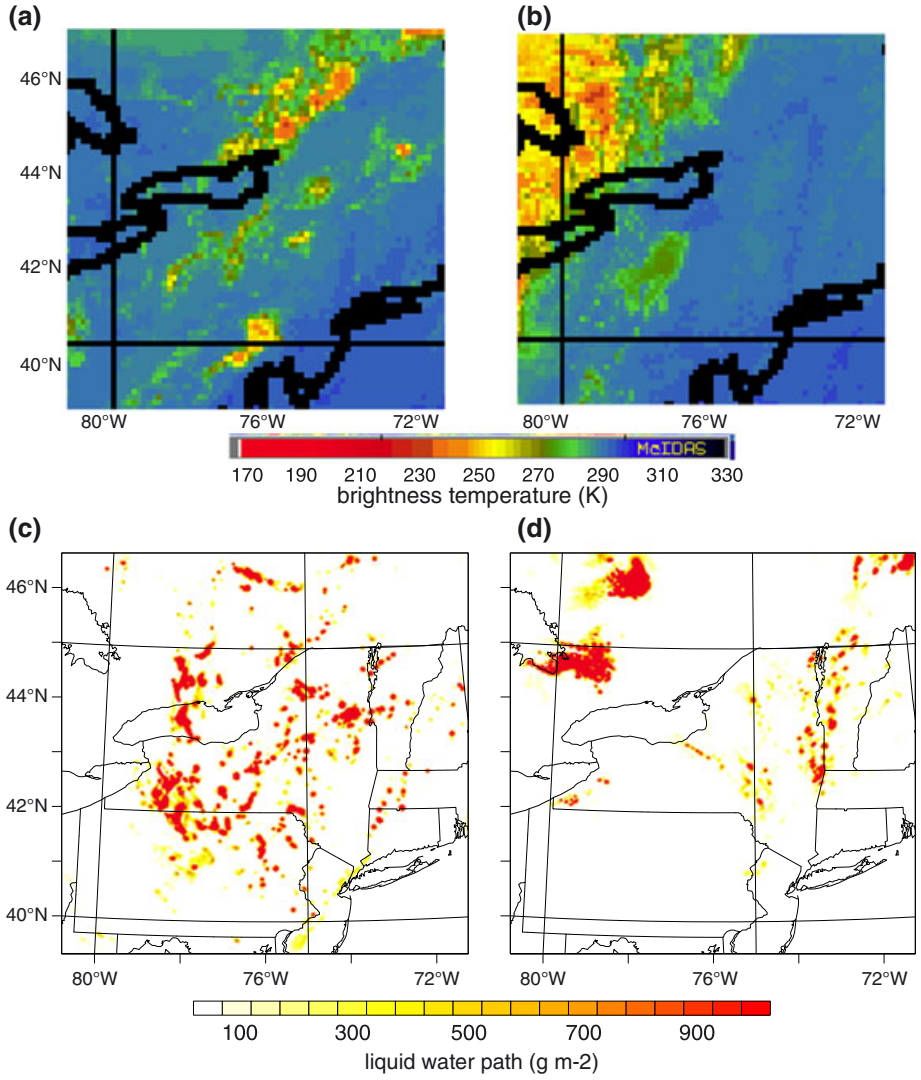

Figure 5. Combined GOES and METEOSAT infrared image at (a) 21 July 2004 00 UTC, and (b) 22 July 2004 06 UTC; column-integrated cloud liquid water and precipitation (units in g m^{-2}) from CAM_driven WRF-Chem simulation at (c) 21 July 2004 00 UTC, and (d) 22 July 2004 06 UTC. Satellite images are from http://www.esrl.noaa.gov/csd/groups/csd4/metproducts/2004icartt/.

Flight 1 took place on 20 July 2004, which was before the WRF-Chem simulation started and the flight path of flight 2 was out of the WRF-Chem analysis domain. The resolution of the WRF-Chem domain also means that the WRF-Chem simulated black carbon profile cannot be directly compared with the measurements of individual flights. Figure 4c illustrates WRF-Chem simulated black carbon concentration averaged over the CAM5 grid (centered at 42.63°N and 75°W) used in Figure 4a. The characteristic of an aloft plume (centered at ~750 hPa) is shown apparently in the WRF-Chem simulated black carbon profile (black line in Figure 4c), implying that the fire plume originating from Alaska and western Canada advected into WRF-Chem domains.

To qualitatively evaluate the simulated convective system, column-integrated cloud liquid water and rain water from WRF-Chem were compared against combined GOES and METEOSAT infrared images (available at http://www.esrl.noaa.gov/csd/groups/csd4/metproducts/2004icartt/) for the entire 2 day period. Figure 5 shows comparisons at 21 July 2004 (0000 UTC) and 22 July 2004 (0600 UTC). Our simulation captured the location and timing of some of the major convection phenomena shown in satellite images, but considerable discrepancies exist between the structure of the simulated and observed convection. For instance, although the WRF-Chem simulation produced relatively strong convective systems over the northwestern

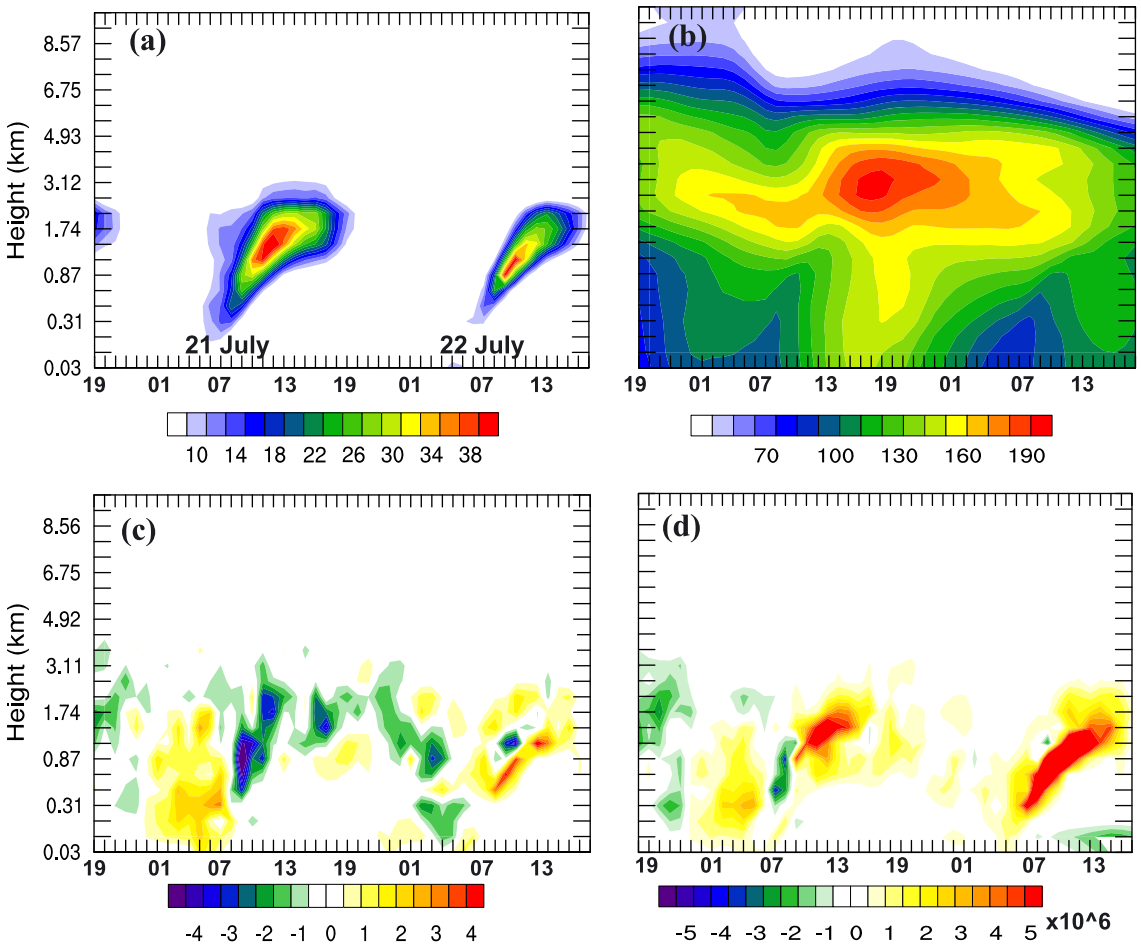

Figure 6. (a) Domain mean cloud liquid water content (CLWC; in mg m^{-3}) from simulation FIRE; (b) differences of domain mean black carbon concentration (mg m^{-3}) in FIRE relative to NoFIRE; (c) difference of domain mean CLWC (in mg m^{-3}) in FIRE relative to NoFIRE; and (d) differences of domain mean cloud droplet number concentration (in # m^{-3}) in FIRE relative to NoFIRE. Horizontal axis is local time 21 and 22 July 2004.

corner of the domain at 0600 UTC on 22 July 2004 (Figure 5d), the spatial extent was much smaller than that shown in the satellite images (Figure 5b). Furthermore, satellite infrared images indicated that these convective systems had a uniform appearance over a relatively large geographical region (Figures 5a and 5b), while WRF-Chem simulated cloud fields were characterized by a heterogeneous cloud deck containing clear areas between the cumulus cells (Figures 5c and 5d). *Otkin and Greenwald* [2008] reported those WRF-simulated cloud fields are strongly influenced by microphysics schemes, with the Lin microphysics scheme tending to produce more heterogeneous cloud fields with clear areas between the cumulus cells compared to other microphysics schemes. Our results are consistent with theirs in that the features shown in our simulated cloud field have similar patchiness (Figures 5c and 5d). While they attributed this deficiency to the Lin microphysics scheme, they also showed that other microphysics schemes outperformed Lin microphysics in reproducing the observed cloud field. More realistic convective systems may be possible with improved microphysics schemes, such as the aforementioned Morrison scheme [*Morrison et al*., 2009].

4.3. Forest Fire Impacts on WRF-Chem Simulation

4.3.1. Fire Plume Impacts on the Convective System

Differences in $PM_{2.5}$ (particulate matter with diameter of 2.5 micrometres or less) total column burden between FIRE and NoFIRE (Figure 1) illustrate that the fire plume advected into the innermost WRF-Chem domain during the simulation period. The domain-mean (i.e., average across the innermost box in Figure 1) cloud liquid water content (CLWC) in Figure 6a shows that for each day of the 2 day simulation period, the cloud system initialized in the early morning at a relatively low altitude (~0.3 km), continued developing and

Table 2. Comparison of Domain-Mean Variables in NoFIRE and FIRE Simulations, and the Percentage Change (Prec_Chg; %), Which was Calculated as the Difference of Each Variable Between the Two Simulations (FIRE -NoFIRE) Divided by That From NoFIRE, for 21 and 22 July 2004[a]

	NoFIRE	FIRE	Percent_Change	NoFIRE	FIRE	Percent_Change
		21 July			22 July	
CLWP	39.1	38.2	−2.3	18.9	19.0	0.5
CDN	4.96e13	5.02e13	1.2	2.88e13	3.02e13	4.9
$N_{COD>1}$	18397	18669	1.5	13078	12941	−1.0
Precip.	6.80	6.16	−9.4	0.92	0.79	−14.1
AOD	0.09	0.26	189	0.12	0.26	117
COD	8.01	8.07	0.7	4.17	4.48	7.4
SWDOWN	454	439	−3.3	476	461	−3.2

[a]Values are presented for daily cloud liquid-water path (CLWP; in g m^{-2}), column-integrated cloud droplet number (CDN; in # m^{-2}), number of grid cells with cloud optical depth greater than 1 ($N_{COD>1}$), accumulated precipitation (Precip.; in mm), aerosol optical depth (AOD), cloud optical depth (COD), and daytime shortwave downwelling radiation at surface (SWDOWN; in W m^{-2}).

reached a daily maximum around midday (altitude between 1 to 2.5 km), and dissipated in the late afternoon. The fire plume resulted in an increase of domain-mean black carbon concentration within ~8 km above ground level. The biggest increase of black carbon concentration occurred approximately 3 km above the ground level (Figure 6b). The fire plume led to a slight increase (up to 5%) in domain mean low-level CLWC prior to the convective period and a slight decrease (up to 8%) in domain mean CLWC within the main cloud system (~0.5 to 3 km) on 21 July 2004 (Figure 6c). On 22 July 2004 there was also a decrease in CLWC within the main cloud system, but an increase below the primary cloud (Figure 6c). For this case the fire plume did not induce significant changes in total cloud liquid-water path (CLWP; Table 2), but rather influenced the vertical distribution of the cloud (increase of lower layer clouds and decrease of upper level clouds). Comparable changes in cloud vertical distribution induced by biomass burning aerosols have been reported in an earlier WRF-Chem study analyzing the impacts of biomass burning over South America [*Wu et al.*, 2011]. *Hill and Dobbie* [2008] also observed this phenomenon when studying the impact of absorbing aerosols in the boundary layer on marine stratocumulus using a Large Eddy Simulation (LES) model.

Signatures of the model physics in Figures 6 and 7 suggest two dominant mechanisms that may have affected the simulated cloud vertical distribution: the plume-induced increases in cloud droplet number concentrations and the thermodynamic changes induced by radiative effects of the fire plume. Our analyses show that high CCN followed the fire plume in both CAM5 and WRF-Chem simulations (figures not shown), which indicates that fire particles, such as black carbon and sulfate aerosols, serve as CCN in this modeling framework. Consequently, the addition of fire particles gave rise to an increase in cloud droplet number concentration (Figure 6d and Table 2). Based on the aerosol-induced increase in cloud droplet number and a smaller relative increase in LWC (Figure 6 and Table 2), a smaller cloud droplet size is inferred via the aerosol first indirect effect [*Twomey*, 1974]. The increase in cloud droplet number concentration and decrease in cloud droplet sizes resulted in more sunlight reflected back to space (the first indirect effect), contributing to a decrease in shortwave radiation reaching the ground and the subsequent cooling close to surface in FIRE relative to NoFIRE (Figure 7a and Table 2).

Comparing Figures 6 and 7 indicates that the thermodynamic changes caused by aerosol radiative effects have also played a role in reducing CLWC in the upper troposphere (and increasing CLWC in the lower troposphere). Figure 7a shows approximately 0.02 K increase in domain-mean daytime temperature coincident with the plume level and a 0.15 K decrease below the plume. These thermodynamic changes resulted in a ~7% decrease in the domain mean convective available potential energy (CAPE) from simulation FIRE relative to NoFIRE during the 2 day analysis period with a maximum reduction of approximately 80 J kg^{-1} around 10:00 UTC on 21 July (Figure 7b), indicating that the atmosphere was more stable in the simulation with the fire plume. Similar findings are reported in previous studies [*Randles and Ramaswamy*, 2010; *Wu et al.*, 2011; *Zhao et al.*, 2012] that biomass burning aerosols cool the surface and warm the local atmosphere where they reside, stabilizing the atmosphere. The CAPE decrease is consistent with the CLWC decrease at the upper troposphere (Figure 6c), as well as the ~10% reduction in accumulated precipitation (Table 2).

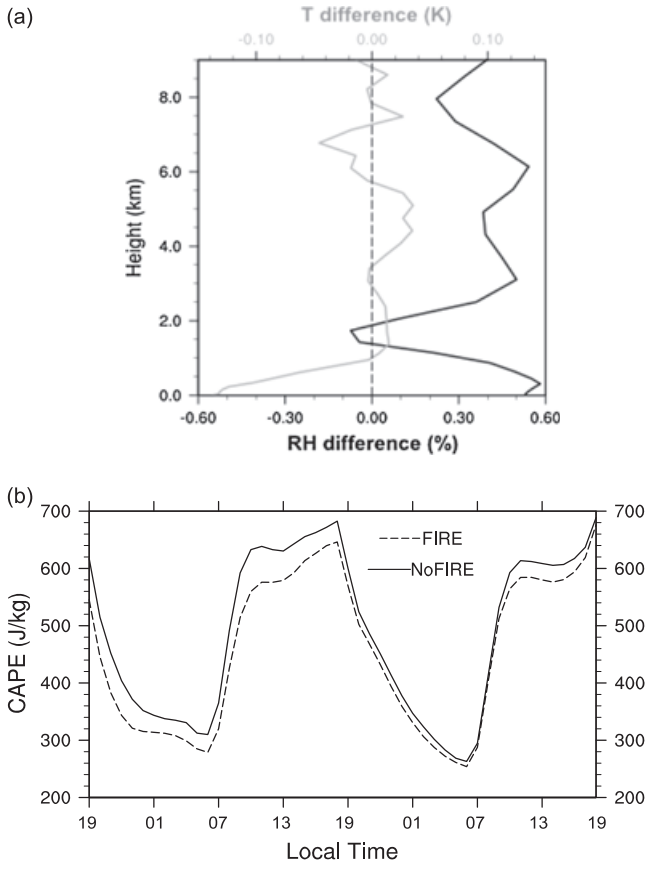

Figure 7. (a) Vertical profiles of differences for domain mean relative humidity (RH; black line) and temperature (*T*; gray line) from FIRE relative to NoFIRE averaged temporally between 6 A.M. to 5 P.M. local time for 21 and 22 July 2004; (b) Time evolution of domain mean CAPE (in J kg^{-1}) from NoFIRE (solid line) and FIRE (dash line) from 20 July 7 P.M. to 22 July 7 P.M.

It is well known that light-absorbing aerosols, such as black carbon and brown carbon, warm the atmosphere where they are suspended due to their optical properties. Both the midlevel heating (Figures 7a) and the aerosol plume (Figure 6b) exist approximately 1–5 km above the ground, suggesting that this midlevel heating is likely due to aerosol direct effect of the light-absorbing aerosols in the fire plume. The midlevel heating and surface cooling can play a role in increasing atmospheric stability, thus inhibiting convection. The decrease in relative humidity (Figure 7a) favors the evaporation of cloud condensates, consistent with the overall CLWC decrease at this level; the more humid environment below ~1.5 km (up to 0.6% increase in relative humidity; Figure 7a) tends to favor cloud formation and the increase in CLWC in the lower troposphere (Figure 6c).

Table 2 summarizes the response of the simulated convection to the addition of lateral aerosol inflow. Changes in daily domain-mean CLWP are within 2.5% despite changes in the cloud vertical distribution (discussion above). The column-integrated cloud droplet number increased by 1.2% and 4.9% for 21 and 22 July 2004, respectively. This is consistent with variations in cloud droplet number concentration shown in Figure 6d. Variations in areas covered with relatively thick clouds (defined as >1 cloud optical depth following *Chapman et al*. [2009]) from the fire plume were insignificant ($<2\%$), although cloud horizontal distribution was altered slightly due to the presence of plumes (not shown). The largest plume-induced changes were for accumulated precipitation, which decreased by 9.5% and 14.1% for 21 and 22 July 2004, respectively, in FIRE compared to NoFIRE (Table 2). Quantitatively, the precipitation reduction signal observed in our study was higher in magnitude than in *Wu et al*. [2011], who showed that 2 day average surface precipitation in the 4 km domain was reduced by 3% in association with local biomass burning emissions over South America. The mechanisms resulting in the reduction in precipitation are discussed in further detail below. Note that aerosol effects are also considered by cloud parameterizations in CAM5, with corresponding effects on the WRF-Chem meteorological boundary conditions in Fire and NoFire. This has the capability of introducing differences at the domain edges because of changes in the CAM5 meteorological fields resulting from aerosol fire emissions and associated feedbacks operating before the point where they reached the WRF-Chem domain. However, comparisons were made for temperature, pressure, and cloud variables along the lateral boundaries between Fire and NoFire, which showed that the differences of meteorological lateral boundary conditions were negligible compared to changes in aerosol loadings along lateral boundaries. Therefore, the variations between different WRF-Chem sensitivity studies discussed in this and the following sections were mostly due to the fire plume aerosols that were transported into the WRF-Chem domain via lateral boundaries, as well as internal convective variability within that domain.

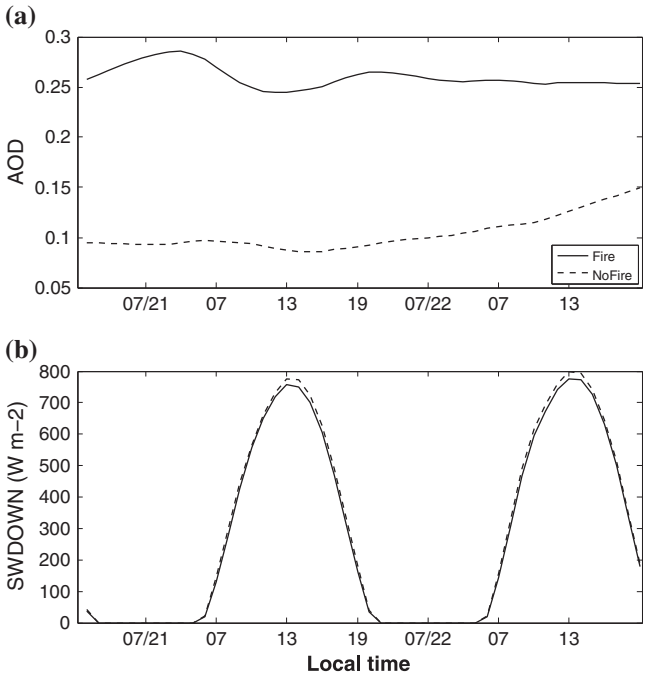

Figure 8. Time evolution of domain mean (a) aerosol optical depth (AOD) and (b) downwelling shortwave radiation at ground surface (SWDOWN; in W m^{-2}) from simulation FIRE (solid line) and NoFIRE (dashed line).

4.3.2. The Fire Plume Impacts on Radiation and Temperature

The domain-mean aerosol optical depth (AOD) nearly tripled from the simulation FIRE compared to that from NoFIRE during the analysis period (Figure 8a). Cloud optical depth (COD) was also increased in FIRE relative to NoFIRE (Table 2) mainly due to plume-induced enhancements in cloud droplet number concentration (Figure 6d). Domain-mean downwelling shortwave radiation at the surface (SWDOWN) was reduced by about 25 W m^{-2} around midday consistent with radiative forcing associated with the fire plume (Figure 8b). The domain-mean daily AOD, COD, and daytime SWDOWN from NoFIRE and FIRE are summarized in Table 2. Changes induced by long-range transported fire plumes in our study (an increase of 0.15 in domain-mean AOD and a decrease of 15 W m^{-2} in domain-mean daytime SWDOWN; Table 2) are quantitatively higher than those shown in *Chapman et al*. [2009], who investigated the radiative impact of local elevated emissions using WRF-Chem over the northeastern United States during the summer of 2004 (9 to 11 August 2004). They demonstrated that by removing all elevated local emissions, the domain-mean AOD was reduced by 0.08, while the daytime mean SWDOWN increased by 5 W m^{-2} during the study's simulation period.

As discussed above in section 4.3.1, the addition of the fire plumes coincided with changes in the vertical structure of the domain mean atmospheric temperature and stability. One hypothesis that we considered (as discussed in section 4.3.1) was that the aerosol shortwave radiative effect produced heating within the aerosol-laden atmospheric layer and cooling below the plume, thereby stabilizing the atmosphere. The vertical cross section plot of the domain mean temperature response (Figure 9a) is consistent with this view. The figure illustrates that from 4 to 10 km, the atmosphere warmed up to 0.2 K consistent with sunlight absorption of black carbon in the upper level fire plume. However, temperature variation was insignificant around cloud levels (~1 to 4 km; Figure 9b). One plausible explanation can be that cooling below the fire plume was counteracted by the release of latent heat associated with the formation of more cloud droplets in FIRE relative to NoFIRE (Figure 6). Furthermore, warming effects of black carbon were obvious only for cloud-free areas, because a large fraction of sunlight was absorbed or reflected back to space by cloud droplets, leaving less sunlight to reach black carbon at cloud level. Consistent with *Zhao et al*. [2012] and *Wu et al*. [2011], a cooling layer existed close to the surface and above the heated layer, respectively. It is logical to infer that the cooling layer close to the surface resulted from less sunlight reaching the ground due to the aerosol layer. We are not able to disentangle the explicit contributions of different physical processes (such as radiation, microphysics, planetary boundary layer) and atmospheric dynamics to the changes in the heating rate because these variables were not saved in the runs we performed. However, we can identify similar scenarios in the literature that exhibit the phenomena observed. For example: *Randles and Ramaswamy* [2010] and *Wu et al*. [2011] attribute the cooling (heating) below (within) the aerosol layer to the radiative effect of the biomass burning aerosols; *Khain et al*. [2005] and *Wang et al*. [2014] demonstrate that aerosol-induced increases in cloud droplets lead to greater release of latent heat. More detailed investigation on these physical mechanisms is needed to identify the causality between aerosols and temperature changes in future studies.

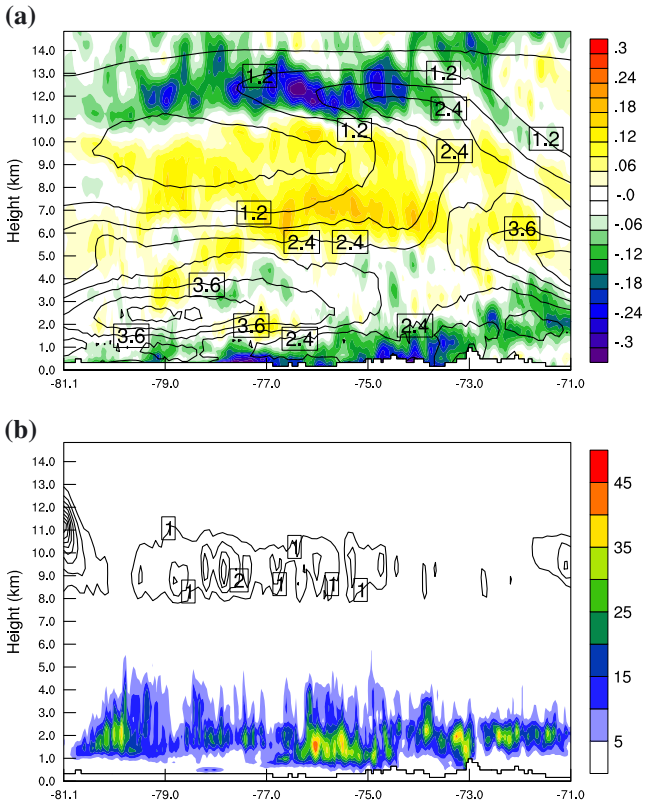

Figure 9. (a) Differences in FIRE simulation relative to NoFIRE simulation for temporal mean (21 and 22 July 2004) temperature (colors; units in °K) and $PM_{2.5}$ concentration (contours; in μg m^{-3}), (b) temporal mean CLWC (colors; in mg m^{-3}) and cloud ice water content (contours, in mg m^{-3}) from NoFIRE simulation along an east-west transect shown in Figure 1.

4.4. Sensitivity Test Isolating Role of Wet Scavenging

The above analysis has emphasized the aerosols' influence on simulated cloud systems. Now, we focus on the influence of convective systems on the simulated aerosol fields through wet scavenging. Using the same strategy as *Zhao et al.* [2012], a sensitivity test simulation was conducted, with wet scavenging turned off (named FIRE_NS) to isolate the effect of particle scavenging by the simulated convective system. All other aspects of the FIRE_NS simulation were identical to FIRE.

Figure 10 depicts overall aerosol scavenging during the 2 day period. Particle scavenging is apparent for nearly the entire domain (Figure 10b), and the domain-mean $PM_{2.5}$ reduced by approximately 23% as a result of particle scavenging. Note that the scavenging discussed here includes both in-cloud and below-cloud scavenging [*Chapman et al.*, 2009]. In-cloud scavenging removes cloud-borne particles using the first-order loss rate of cloud water, while below-cloud scavenging washes out aerosols by impaction and interception. Only about 25% of the $PM_{2.5}$ mass reduction occurred below a 1 km altitude when averaged temporally over the simulation period, implying that wet removal of aerosols in our simulations was likely dominated by in-cloud scavenging because the maximum cloud base was approximately 1 km (Figure 6a).

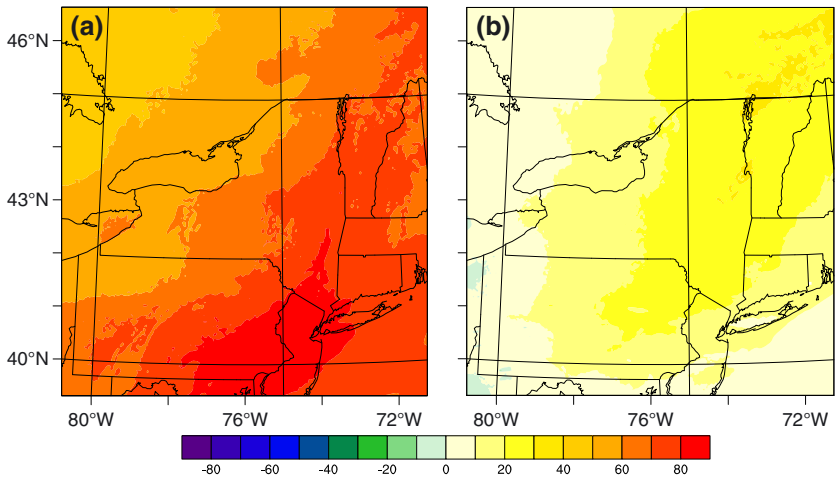

Figure 10. Spatial distribution of 2 day mean (a) column-integrated $PM_{2.5}$ concentration (mg m^{-2}) from FIRE_NS case and (b) differences of column-integrated $PM_{2.5}$ concentration (mg m^{-2}) for the FIRE_NS case relative to the FIRE case.

Table 3. Concentrations of Black Carbon and Other Aerosols on Lateral Boundaries of WRF-Chem Outermost Domain in Three Sensitivity Simulations Compared to Simulation FIRE

	DoubleBC	HalfBC	DoublePlume
Black carbon	double	Half	double
Other aerosols	unchanged	unchanged	double

Wet scavenging is part of a two-way interaction between the convective system and aerosols. On one hand, scavenging incurred a decrease in aerosol mass (discussed above); on the other hand, variations in aerosol loadings affected the convective system. For instance, one effect of turning off wet scavenging was a repartitioning of more domain mean condensate in liquid form and less condensate in ice form. The 2 day domain-mean cloud water and rain water in simulation FIRE_NS increased by 5% and 3%, respectively, relative to simulation FIRE; while cloud ice, snow, and graupel in simulation FIRE_NS decreased by 6%, 4%, and 1%, respectively, over simulation FIRE. Another effect of turning off wet scavenging was reduced rainfall. The 2 day accumulated precipitation in simulation FIRE_NS was about 3% over that in simulation FIRE. These sensitivities likely result from aerosol forcing. For instance, the repartitioning of condensate can be related to radiative heating of ice hydrometeors. As discussed above, adding fire plumes produced a 0.02 K increase of domain-mean temperature between 5 and 10 km, i.e., in the middle to upper troposphere where most simulated ice hydrometeors exist (Figure 9b). A plausible hypothesis can then be that more ice hydrometeors (ice cloud, snow, and graupel) melted to liquid form (cloud and rain water) in FIRE_NS comparing to FIRE due to higher plume intensity in FIRE_NS than FIRE. This perhaps also contributed to the overall increase (~3%) in surface precipitation.

4.5. Sensitivity Tests Varying Plume Magnitude and Composition

Previous observational studies [*Ramanathan and Carmichael*, 2008; *Ramana et al.*, 2010] have shown that atmospheric warming induced by black carbon depends not only on the concentration of black carbon but also on ratios of black carbon to other aerosols, such as sulfate. Atmospheric responses to different ratios of black carbon to other aerosols in the fire plume, as well as to different overall plume intensities, are explored in this section. Three sensitivity simulations were carried out by modifying concentrations of black carbon (and other aerosols) on WRF-Chem lateral boundaries of the outermost domain (Table 3), which were derived from CAM_GFED results using the CAM5/WRF-Chem interface described previously.

Black carbon constituted only a small fraction of the fire plume in the control case, so varying the concentration of black carbon while keeping concentrations of other aerosols unchanged (DoubleBC and

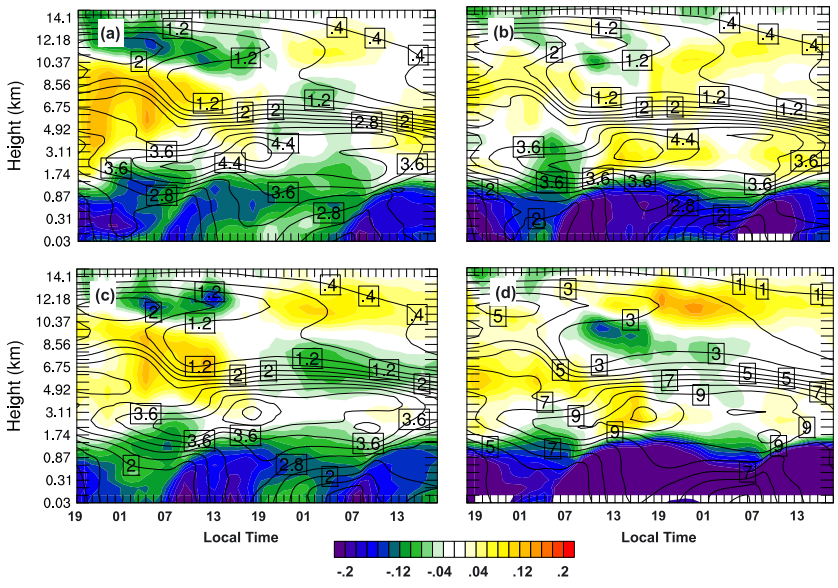

Figure 11. Differences of domain mean temperature (colors; in °K) and $PM_{2.5}$ concentration (contours; in μg m^{-3}) in (a) FIRE relative to NoFIRE, (b) DoubleBC relative to NoFIRE, (c) HalfBC relative to NoFIRE, and (d) DoublePlume relative to NoFIRE.

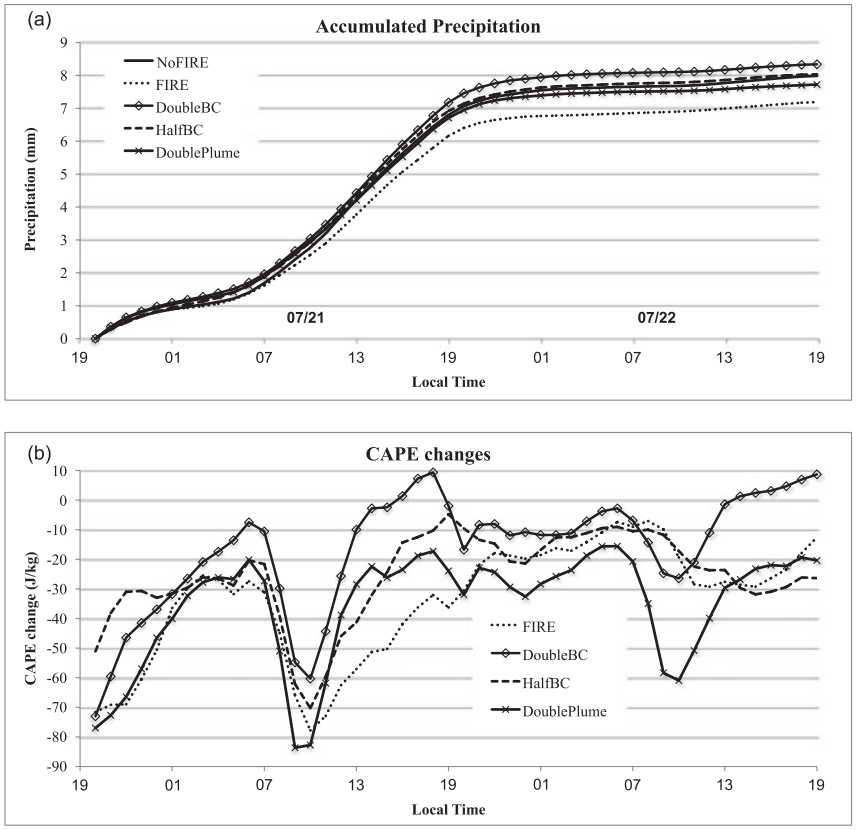

Figure 12. Time evolution of (a) domain-mean accumulated precipitation (mm) from different WRF-Chem simulations and (b) domain-mean CAPE changes (J kg^{-1}) from simulation FIRE, DoubleBC, HalfBC, and DoublePlume relative to NoFIRE.

HalfBC) did not lead to significant changes in the domain mean $PM_{2.5}$ anomalies (Figures 11b and 11c) compared to FIRE (Figure 11a). However, changes in the ratio of black carbon to other plume aerosols induced different responses in atmospheric temperature. Although the maximum magnitude of induced temperature enhancement was smaller in DoubleBC (Figure 11b) compared to FIRE (Figure 11a), a thicker layer was heated in DoubleBC (Figure 11b) relative to FIRE (Figure 11a) for most of the simulation period. The cooling above the heated layer, which was evident between ~10 to 14 km for the first half of the simulation period in FIRE (Figure 11a), was insignificant in DoubleBC (Figure 11b).

On the other hand, Figure 11 clearly shows that cooling close to the surface is a very robust effect of aerosol forcing. Low-level cooling was intensified significantly in DoubleBC (Figure 11b) compared to FIRE (Figure 11a), as more solar radiation was absorbed due to the increase in black carbon concentration. Consistently, cutting black carbon by half (HalfBC; Figure 11c) led to less-significant low-level cooling. Cooling close to the surface was most significant in DoublePlume (Figure 11d), which was expected since overall aerosol concentration was almost doubled in this simulation (Figure 11d) compared to the other three simulations (Figures 11a–11c). Both absorbing and scattering aerosols contributed to surface cooling. In summary, the thermodynamic changes in this sensitivity test show clearly that near-surface atmospheric temperature is sensitive both to the ratio of black carbon to other aerosols and especially to plume concentration.

Changes in black carbon concentration and overall plume concentration also led to variations in the simulated convective system. Figure 12 illustrates the evolution of domain-mean accumulated precipitation and CAPE changes from different simulations relative to NoFIRE. Simulation FIRE led to about a 10% reduction in precipitation compared to NoFIRE, which we have pointed out could be viewed as a consequence of the plume-induced increase in atmospheric stability and the associated decrease in autoconversion rates for cloud droplets to form rain droplets (see section 4.3.1). Interestingly, when the overall plume concentration

was doubled (DoublePlume), precipitation suppression was less noticeable (Figure 12a; a reduction of 3% in 2 day accumulated precipitation relative to NoFIRE). One possible reason can be that, even though surface cooling was enhanced in DoublePlume relative to FIRE because of the increased plume intensity, the atmosphere immediately above the surface cooling layer was heated less in DoublePlume compared to that in FIRE (Figures 11d versus 11a). Thus, the overall increase in atmospheric stability relative to NoFIRE can be smaller in DoublePlume than that in FIRE within the convective layer. This was consistent with the CAPE variations (Figure 12b), which show that the FIRE simulation resulted in the biggest CAPE reduction relative to NoFIRE during the convective period when most of the precipitation occurred (0500 to 1900 local standard time (LST) on 21 July 2004). The domain-mean CAPE reduction (relative to NoFIRE) averaged over this convective period was −47.3, −17.4, −34.0, and −37 J kg^{-1} for FIRE, DoubleBC, HalfBC, and DoublePlume, respectively. DoubleBC led to the least CAPE reduction compared to other simulations (Figure 12b). Furthermore, DoubleBC led to a temperature increase for almost the entire atmosphere above 2 km for most of the simulation period (Figure 11b), facilitating the melting of ice hydrometeors to liquids, which might be the primary cause of the 4% increase in surface precipitation from DoubleBC compared to NoFIRE (Figure 12a).

The divergent precipitation responses in twin experiments with modifications in aerosol forcing illustrate variability similar to that reported by *Morrison and Grabowski* [2011]. These types of interaction between convective systems and aerosols are clearly complex. *Ntelekos et al*. [2009] used WRF-Chem in a similar study region and found precipitation was enhanced for some cells and inhibited in other cells, likely because of variability in anthropogenic aerosol loading as well as to the internal variability intrinsic to atmospheric moist thermodynamics at convection resolving scales. The CAPE reduction in all sensitivity runs with fire plume relative to NoFIRE (Figure 12b) suggests that the plume-induced CAPE reduction were applicable to a wide range of conditions.

5. Summary

A globally driven regional modeling system, which coupled aerosol-enabled CAM5 and WRF-Chem, was used to explore the meteorological impacts of wildfire emissions over Alaska and western Canada when they are transported over the northeastern United States during the summer of 2004. Daily forest fire emissions were implemented into CAM5 by vertically distributing GFEDv3 fire emissions among the CAM5 vertical layers. Nudging was applied to CAM5 in order to observationally constrain the global simulations. The fire emissions in CAM5 were transported to the WRF-Chem domain where they influenced the simulated meteorology in the convection-resolving WRF-Chem domain (with 3 km horizontal resolution). Regional climate simulations conventionally driven by reanalysis data and GCTMs are not able to simulate future climate scenarios, because both reanalysis data and GCTMs depend on observed dynamics. The purpose of developing this modeling framework is not to improve conventional regional climate simulations but to establish a framework that can be applied to explore regional meteorological and air quality impacts of global-scale perturbations in meteorological conditions and emissions decades into the future. In this paper, nudging in CAM5 is used to constrain observed meteorology to evaluate a test case, but in future work nudging can be removed to investigate the effects of global-scale changes in emissions and climate on regional weather and air quality.

CAM5 and WRF-Chem substantially underestimated the black carbon profile relative to in situ observations collected by the NASA DC-8 aircraft during the ICARTT field campaign, primarily due to the coarse spatial and temporal resolution of CAM5, transport physics in CAM5, and a known low bias in GFEDv3 fire emissions. WRF-Chem simulated cloud water and rain water had timings and locations similar to those seen in GOES infrared images; however, the simulations produced smaller spatial extent than observations. Results from the modeling framework were compared with WRF-Chem results driven by NARR reanalysis. The NARR_driven and CAM5_driven WRF-Chem results were consistent overall, indicating that the coupling of the two models provided a way to drive a finer-resolution regional model with CAM5.

After transport to the innermost WRF-Chem domain with explicit convection, an initial pair of experiments suggested that biomass burning aerosols led to some variations in cloud vertical distribution (a CLWC increase below the main plume and CLWC decrease where the plume encountered clouds). The comparison between two sets of WRF-Chem simulations, one with both aerosol direct and indirect effects activated

and the other with only aerosol indirect effects activated, implied that the aerosol indirect effect and direct effect had opposite impacts on the cloud system: the aerosol indirect effect likely resulted in an overall CLWC increase due to plume-induced enhancement in cloud droplet number concentration, while the thermodynamic change of the atmosphere induced by the aerosol direct effect cooled the surface and enhanced atmospheric stability (a 8.6% decrease in domain mean CAPE during the main convective period from FIRE relative to NoFIRE), leading to a CLWC reduction in the upper troposphere (above ~0.5 km). Despite changes in cloud vertical distribution, the fire plume resulted in only marginal CLWP variations (<2.5%). The fire plume resulted in 9.5% and 14.1% decreases in accumulated surface precipitation for 21 and 22 July 2004, respectively. The plume also led to almost tripled AOD, and about a 25 W m^{-2} decrease in SWDOWN around midday.

The convective system scavenged about 23% of plume aerosols, mostly through in-cloud scavenging. The higher loading of black carbon in the simulation without wet scavenging further heated the atmosphere, resulting in an increase in liquid hydrometeors and a decrease in ice hydrometeors relative to the simulation with wet scavenging. The melting of ice hydrometeors to liquid form likely played a more important role in affecting surface precipitation than the weakening of the convection due to the aerosol direct effect and the decrease in autoconversion rate from cloud droplets to rain droplets due to aerosol indirect effects. This then resulted in a slight (~3%) increase in 2 day accumulated surface precipitation in the WRF-Chem simulation without wet scavenging relative to the simulation with wet scavenging.

Using this modeling framework, another suite of simulations was carried out with varying ratios of black carbon to overall plume concentrations in order to explore the sensitivity of the above atmospheric responses. The most robust effect of the nonlocal aerosol forcing identified across this ensemble was a cooling of the lower atmosphere, which scaled approximately with variations in the plume magnitude and composition. The plume-induced CAPE decreases were also likely to be representative of a range of conditions based on this ensemble. Convection was affected by changes in plume or black carbon concentration, although this response did not scale cleanly as a function of aerosol forcing in different simulations.

Acknowledgments

This study was supported by the Department of Energy (DOE) grant DE-SC0002003. The authors thank Steven Ghan, Minghuai Wang, Jerome Fast, and Richard Easter of Pacific Northwest National Laboratory, as well as Jerry Olson and Dave Williamson from the National Center for Atmospheric Research for valuable input. Our gratitude goes to Georg Grell, Steven Peckham, and the WRF support staff for their assistance with WRF-Chem model. Queen Bee at the Louisiana Optical Network Initiative and Steele at Purdue University provided computing resources from the National Science Foundation (NSF) through XSEDE allocation TG-ATM090002. Triton Resources at the San Diego Supercomputer Center provided computer clusters for the model simulations. Finally, G.J.K., M.S.P., and R.C.J.S. acknowledge support from the Center for Multiscale Modeling of Atmospheric Processes (CMMAP), an NSF Science and Technology Center managed by Colorado State University under cooperative agreement ATM-0425247.

References

Albrecht, B. A. (1989), Aerosols, cloud microphysics, and fractional cloudiness, *Science*, *245*, 1227–1230, doi:10.1126/science.245.4923.1227.

Boyle, J. S., D. Williamson, R. Cederwall, M. Fiorino, J. Hnilo, J. Olson, T. Phillips, G. Potter, and S. Xie (2005), Diagnosis of Community Atmospheric Model 2 (CAM2) in numerical weather forecast configuration at Atmospheric Radiation Measurement sites, *J. Geophys. Res.*, *110*, D15S15, doi:10.1029/2004JD005042.

Chapman, E. G., W. I. Gustafson Jr., R. C. Easter, J. C. Barnard, S. J. Ghan, M. S. Pekour, and J. D. Fast (2009), Coupling aerosol-cloud-radiative processes in the WRF-Chem model: Investigating the radiative impact of elevated point sources, *Atmos. Chem. Phys.*, *9*, 945–964, doi:10.5194/acp-9-945-2009.

Chow, J. C., J. G. Watson, P. Doraiswamy, L.-W. A. Chen, D. A. Sodeman, D. H. Lowenthal, K. Park, W. P. Arnott, and N. Motallebi (2009), Aerosol light absorption, black carbon and elemental carbon at the Fresno Supersite, California, *Atmos. Res.*, *93*, 874–887, doi:10.1016/j.atmosres.2009.04.010.

Colarco, P. R., M. R. Schoeberl, B. G. Doddridge, L. T. Marufu, O. Torres, and E. J. Welton (2004), Transport of smoke from Canadian forest fires to the surface near Washington, D. C.: Injection height, entrainment, and optical properties, *J. Geophys. Res.*, *109*, D06203, doi:10.1029/2003JD004248.

Crutzen, P., and M. Andreae (1990), Biomass burning in the tropics: Impact on atmospheric chemistry and biogeochemical cycles, *Science*, *250*, 1669–1678.

Dee, D. P., et al. (2011), The ERA-Interim reanalysis: Configuration and performance of the data assimilation system, *Q. J. R. Meteorol. Soc.*, *137*(656), 553–597.

Fast, J. D., W. I. Gustafson Jr., R. C. Easter, R. A. Zaveri, J. C. Barnard, E. G. Chapman, G. A. Grell, and S. E. Peckham (2006), Evolution of ozone, particulates, and aerosol direct radiative forcing in the vicinity of Houston using a fully coupled meteorology-chemistry-aerosol model, *J. Geophys. Res.*, *111*, D21305, doi:10.1029/2005JD006721.

Fast, J. D., et al. (2009), Evaluating simulated primary anthropogenic and biomass burning organic aerosols during MILAGRO: Implications for assessing treatments of secondary organic aerosols, *Atmos. Chem. Phys.*, *9*, 6196–6215.

Fehsenfeld, F. C., et al. (2006), International Consortium for Atmospheric Research on Transport and Transformation (ICARTT): North America to Europe—Overview of the 2004 summer field study, *J. Geophys. Res.*, *111*, D23S01, doi:10.1029/2006JD007829.

Ghan, S. J., L. R. Leung, R. C. Easter, and H. Abdul-Razzak (1997), Prediction of droplet number in a general circulation model, *J. Geophys. Res.*, *102*, 21,777–21,794, doi:10.1029/97JD01810.

Giglio, L., et al. (2010), Assessing variability and long-term trends in burned area by merging multiple satellite fire products, *Biogeosciences*, *7*(3), 1171–1186.

Grell, G. A., and D. Devenyi (2002), A generalized approach to parameterizing convection combining ensemble and data assimilation techniques, *Geophys. Res. Lett.*, *29*(14), 1693, doi:10.1029/2002GL015311.

Grell, G. A., S. E. Peckham, R. Schmitz, S. A. McKenn, G. Frost, W. C. Skamarock, and B. Eder (2005), Fully coupled "online" chemistry within the WRF model, *Atmos. Environ.*, *39*, 6957–6975, doi:10.1016/j.atmosenv.2005.04.027.

Grell, G. A., S. R. Freitas, M. Stuefer, and J. D. Fast (2011), Inclusion of biomass burning in WRF-Chem: Impact on wildfires on weather forecasts, *Atmos. Chem. Phys.*, *11*, 5289–5303.

Guenther, A. B., P. R. Zimmerman, P. C. Harley, R. K. Monson, and R. Fall (1993), Isoprene and monoterpene emission rate variability: Model evaluations and sensitivity analyses, *J. Geophys. Res.*, *98D*, 12,609–12,617, doi:10.1029/93JD00527.

Hill, A. A., and S. Dobbie (2008), The impact of aerosols on non-precipitating marine stratocumulus. II: The semi-direct effect, *Q. J. R. Meteorol. Soc.*, *134*(634), 1155–1165, doi:10.1002/qj.277.

Huang, M., et al. (2010), Impacts of transported background ozone on California air quality during the ARCTAS-CARB period—A multi-scale modeling study, *Atmos. Chem. Phys.*, *10*, 6947–6968, doi:10.5194/acp-10-6947-2010.

Intergovernmental Panel on Climate Change: Climate Change 2007 (2007), The physical science basis, in *Contribution of Working Group I to the Fourth Assessment Report of the Intergovernmental Panel on Climate Change*, edited by S. Solomon et al., pp. 996, Cambridge Univ. Press, Cambridge, and New York.

Kaufman, Y. J., and R. S. Fraser (1997), The effect of smoke particles on clouds and climate forcing, *Science*, *277*, 1636–1639.

Khain, A., D. Rosenfeld, and A. Pokrovsky (2005), Aerosol impact on the dynamics and microphysics of convective clouds, *Q. J. R. Meteorol. Soc.*, *131*, 2639–2663.

Kooperman, G. J., M. S. Pritchard, S. J. Ghan, M. Wang, R. C. J. Somerville, and L. M. Russell (2012), Constraining the influence of natural variability to improve estimates of global aerosol indirect effects in a nudged version of the Community Atmosphere Model 5, *J. Geophys. Res.*, *117*, D23204, doi:10.1029/2012JD018588.

Lamarque, J. F., et al. (2010), Historical (1850–2000) gridded anthropogenic and biomass burning emissions of reactive gases and aerosols: Methodology and application, *Atmos. Chem. Phys.*, *10*, 7017–7039, doi:10.5194/acp-10-7017-2010.

Lewis, E. R., and S. E. Schwartz (2004), *Sea Salt Aerosol Production: Mechanisms, Methods, Measurements and Models*, *Geophys. Monogr. Ser.*, vol. 152, pp. 413, AGU, Washington, D. C.

Lin, M., T. Holloway, G. R. Carmichael, and A. M. Fiore (2010), Quantifying pollution inflow and outflow over East Asia in spring with regional and global models, *Atmos. Chem. Phys.*, *10*, 4221–4239, doi:10.5194/acp-10-4221-2010.

Lin, Y.-L., R. D. Farley, and H. D. Orville (1983), Bulk parameterization of the snow field in a cloud model, *J. Climate Appl. Meteorol.*, *22*, 1065–1092.

Liu, S. C., et al. (1996), Model study of tropospheric trace species distributions during PEM-West A, *J. Geophys. Res.*, *101*, 2073–26,583, doi:10.1029/95JD02277.

Liu, X., et al. (2012), Toward a minimal representation of aerosols in climate models: Description and evaluation in the community atmosphere model CAM5, *Geosci. Model Dev.*, *5*, 709–739, doi:10.5194/gmd-5-709-2012.

Liu, Y., P. H. Daum, and R. McGraw (2005), Size truncation effect, thresh- old behavior, and a new type of autoconversion parameterization, *Geophys. Res. Lett.*, *32*, L11811, doi:10.1029/2005GL022636.

McMillan, W. W., et al. (2008), AIRS views transport from 12 to 22 July 2004 Alaskan/Canadian fires: Correlation of AIRS CO and MODIS AOD with forward trajectories and comparison of AIRS CO retrievals with DC-8 in situ measurements during INTEX-A/ICARTT, *J. Geophys. Res.*, *113*, D20301, doi:10.1029/2007JD009711.

Mesinger, F., et al. (2006), North American regional reanalysis, *Bull. Am. Meteorol. Soc.*, *87*, 343–360.

Morrison, H., and A. Gettelman (2008), A new two-moment bulk stratiform cloud microphysics scheme in the community atmosphere model, version 3 (CAM3). Part I: Description and numerical tests, *J. Clim.*, *21*(15), 3642–3659.

Morrison, H., and W. W. Grabowski (2011), Cloud-system resolving model simulations of aerosol indirect effects on tropical deep convection and its thermodynamic environment, *Atmos. Chem. Phys.*, *11*, 10,503–10,523, doi:10.5194/acp-11-10503-2011.

Morrison, H., G. Thompson, and V. Tatarskii (2009), Impact of cloud microphysics on the development of trailing stratiform precipitation in a simulated squall line: Comparison of one- and two-moment schemes, *Mon. Weather Rev.*, *137*, 991–1007, doi:10.1175/2008MWR2556.1.

Mu, M., et al. (2011), Daily and 3-hourly variability in global fire emissions and consequences for atmospheric model predictions of carbon monoxide, *J. Geophys. Res.*, *116*, D24303, doi:10.1029/2011JD016245.

Neale, R. B., et al. (2010), NCAR technical note: Description of the NCAR Community Atmosphere Model (CAM 5.0), National Center for Atmospheric Research, Boulder.

Ntelekos, A. A., J. A. Smith, L. J. Donner, J. D. Fast, W. I. Gustafson Jr., E. G. Chapman, and W. F. Krajewski (2009), The effects of aerosols on intense convective precipitation in the northeastern US, *Q. J. R. Meteorol. Soc.*, *135*, 1367–1391.

Otkin, J. A., and T. J. Greenwald (2008), Comparison of WRF model-simulated and MODIS-derived cloud data, *Mon. Weather Rev.*, *136*, 1957–1969.

Park, S., and C. S. Bretherton (2009), The university of Washington shallow convection and moist turbulence schemes and their impact on climate simulations with the community atmosphere model, *J. Clim.*, *22*(12), 3449–3469.

Penner, J. E., R. E. Dickinson, and C. A. O'Neill (1992), Effects of aerosol from biomass burning on the global radiation budget, *Science*, *256*, 1432–1434.

Pfister, G., P. G. Hess, L. K. Emmons, J.-F. Lamarque, C. Wiedinmyer, D. P. Edwards, G. Pe´tron, J. C. Gille, and G. W. Sachse (2005), Quantifying CO emissions from the 2004 Alaskan wildfires using MOPITT CO data, *Geophys. Res. Lett.*, *32*, L11809, doi:10.1029/2005GL022995.

Pfister, G., et al. (2011), Characterizing summertime chemical boundary conditions for airmasses entering the US West Coast, *Atmos. Chem. Phys.*, *11*, 1769–1790, doi:10.5194/acp-11-1769-2011.

Pfister, G. G., P. G. Hess, L. K. Emmons, P. J. Rasch, and F. M. Vitt (2008), Impact of the summer 2004 Alaska fires on top of the atmosphere clear-sky radiation fluxes, *J. Geophys. Res.*, *113*, D02204, doi:10.1029/2007JD008797.

Ramana, M. V., V. Ramanathan, Y. Feng, S.-C. Yoon, S.-W. Kim, G. Carmichael, and J. J. Schauer (2010), Warming influenced by the ratio of black carbon to sulphate and the black-carbon source, *Nat. Geosci.*, *3*, 542–545.

Ramanathan, V., and G. Carmichael (2008), Global and regional climate changes due to black carbon, *Nat. Geosci.*, *1*, 221–227.

Randles, C. A., and V. Ramaswamy (2010), Direct and semi-direct impacts of absorbing biomass burning aerosol on the climate of southern Africa: A Geophysical Fluid Dynamics Laboratory GCM sensitivity study, *Atmos. Chem. Phys.*, *10*(20), 9819–9831, doi:10.5194/acp-10-9819-2010.

Ritchie, E. A., and R. L. Elsberry (2007), Simulations of the extra- tropical transition of tropical cyclones: Phasing between the upper-level trough and tropical cyclones, *Mon. Weather Rev.*, *135*, 862–876.

Roberts, G. C., A. Nenes, J. H. Seinfeld, and M. O. Andreae (2003), Impact of biomass burning on cloud properties in the Amazon Basin, *J. Geophys. Res.*, *108*(D2), 4062, doi:10.1029/2001JD000985.

Saide, P. E., et al. (2012), Evaluating WRF-Chem aerosol indirect effects in Southeast Pacific marine stratocumulus during VOCALS-REx, *Atmos. Chem. Phys.*, *12*, 3045–3064, doi:10.5194/acp-12-3045-2012.

Seiler, W., and P. J. Crutzen (1980), Estimates of gross and net fluxes of carbon between the biosphere and the atmosphere from biomass burning, *Clim. Change*, *2*, 207–247.
Sessions, W. R., H. E. Fuelberg, R. A. Kahn, and D. M. Winker (2010), An investigation of methods for injecting emissions from boreal wildfires using WRF-Chem during ARCTAS, *Atmos. Chem. Phys. Discuss.*, *10*, 26,551–26,606, doi:10.5194/acpd-10-26551-2010.
Skamarock, W. C., J. B. Klemp, J. Dudhia, D. O. Gill, D. M. Barker, M. G. Duda, X.-Y. Huang, W. Wang, and J. G. Powers (2008), A description of the advanced research WRF version 3, *Tech. Note NCAR/TN-475+STR*, 125 pp., Natl. Cent. for Atmos. Res., Boulder, Colo. [Available at http://www.mmm.ucar.edu/wrf/users/docs/arw_v3.pdf.]
Stohl, A., et al. (2006), Pan-Arctic enhancements of light absorbing aerosol concentrations due to North American boreal forest fires during summer 2004, *J. Geophys. Res.*, *111*, D22214, doi:10.1029/2006JD007216.
Stroppiana, D., P. A. Brivio, J.-M. Grégoire, C. Liousse, B. Guillaume, C. Granier, A. Mieville, M. Chin, and G. Pétron (2010), Comparison of global inventories of CO emissions from biomass burning derived from remotely sensed data, *Atmos. Chem. Phys.*, *10*, 12,173–12,189, doi:10.5194/acp-10-12173-2010.
Tang, Y., et al. (2004), Multiscale simulations of tropospheric chemistry in the eastern Pacific and on the U.S. West Coast during spring 2002, *J. Geophys. Res.*, *109*, D23S11, doi:10.1029/2004JD004513.
Turquety, S., et al. (2007), Inventory of boreal fire emissions for North America in 2004: Importance of peat burning and pyroconvective injection, *J. Geophys. Res.*, *112*, D12S03, doi:10.1029/2006JD007281.
Twomey, S. (1974), Pollution and the planetary albedo, *Atmos. Environ.*, *8*, 1251–1256.
Val Martin, M., J. A. Logan, R. A. Kahn, F.-Y. Leung, D. L. Nelson, and D. J. Diner (2010), Smoke injection heights from fires in North America: Analysis of 5 years of satellite observations, *Atmos. Chem. Phys.*, *10*, 1491–1510.
Van der Werf, G. R., J. T. Randerson, L. Giglio, G. J. Collatz, M. Mu, P. S. Kasibhatla, D. C. Morton, R. S. DeFries, Y. Jin, and T. T. van Leeuwen (2010), Global fire emissions and the contribution of deforestation, savanna, forest, agricultural, and peat fires (1997–2009), *Atmos. Chem. Phys.*, *10*, 11,707–11,735.
Wang, Y., K.-H. Lee, Y. Lin, M. Levy, and R. Zhang (2014), Distinct effects of anthropogenic aerosols on tropical cyclones, *Nat. Clim. Change*, *4*, doi:10.1038/nclimate2144.
Warneke, C., et al. (2006), Biomass burning and anthropogenic sources of CO over New England in the summer 2004, *J. Geophys. Res.*, *111*, D23S15, doi:10.1029/2005JD006878.
Winner, D. A., G. R. Cass, and R. A. Harley (1995), Effect of alternative boundary conditions on predicted ozone control strategy: A case study in Los Angeles area, *Atmos. Environ.*, *29*(33), 3451–3464, doi:10.1016/1352-2310(95)00222-K.
Wotawa, G., and M. Trainer (2000), The influence of Canadian forest fires on pollutant concentrations in the United States, *Science*, *288*, 324–328.
Wu, L., H. Su, and J. H. Jiang (2011), Regional simulations of deep convection and biomass burning over South America. Part II: Biomass burning aerosol effects on clouds and precipitation, *J. Geophys. Res.*, *116*, D17209, doi:10.1029/2011JD016106.
Zangvil, A., and P. Druian (1990), Upper air trough axis orientation and the spatial distribution of rainfall over Israel, *Int. J. Climatol.*, *10*, 57–62.
Zhang, G. J., and N. A. McFarlane (1995), Sensitivity of climate simulations to the parameterization of cumulus convection in the Canadian climate center general-circulation model, *Atmos.–Ocean*, *33*(3), 407–446.
Zhao, C., X. Liu, L. R. Leung, B. Johnson, S. McFarlane, W. I. Gustafson Jr., J. D. Fast, and R. Easter (2010), The spatial distribution of dust and its short wave radiative impact over North Africa: Modeling sensitivity to dust emissions and aerosol size treatments, *Atmos. Chem. Phys.*, *10*, 8821–8838.
Zhao, Z., S.-H. Chen, M. J. Kleeman, M. Tyree, and D. Cayan (2011), The impact of climate change on Air quality–related meteorological conditions in California. Part I: Present time simulation analysis, *J. Clim.*, *24*, 3344–3361, doi:10.1175/2011JCLI3849.1.
Zhao, Z., M. S. Pritchard, and L. M. Russell (2012), Effects on precipitation, clouds, and temperature from long-range transport of idealized aerosol plumes in WRF-Chem simulations, *J. Geophys. Res.*, *117*, D05206, doi:10.1029/2011JD016744.